
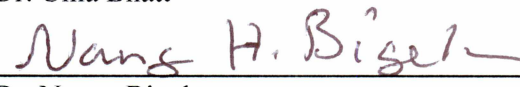


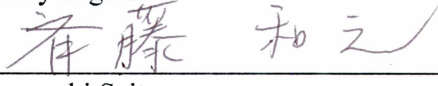
LATE QUATERNARY AND FUTURE BIOME SIMULATIONS
FOR ALASKA AND EASTERN RUSSIA

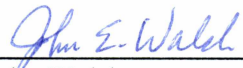
By

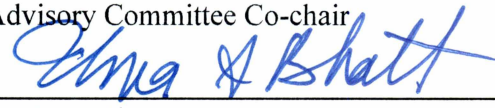
Amy S. Hendricks


RECOMMENDED: 
Dr. Uma Bhatt

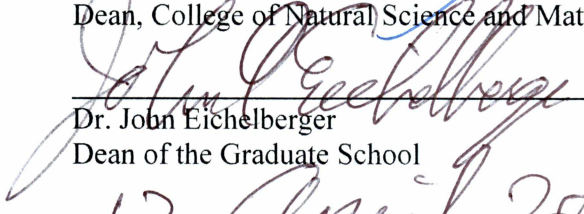

Dr. Nancy Bigelow


Dr. Kazuyuki Saito
Advisory Committee Co-chair


Dr. John Walsh
Advisory Committee Co-chair


Dr. Uma Bhatt
Chair, Department of Atmospheric Sciences

APPROVED: 
Dr. Paul Layer
Dean, College of Natural Science and Mathematics


Dr. John Eichelberger
Dean of the Graduate School

12 April 2016
Date

LATE QUATERNARY AND FUTURE BIOME SIMULATIONS
FOR ALASKA AND EASTERN RUSSIA

A
THESIS

Presented to the Faculty
of the University of Alaska Fairbanks

in Partial Fulfillment of the Requirements
for the Degree of

MASTER OF SCIENCE

By

Amy S. Hendricks, B.S.

Fairbanks, AK

May 2016

Abstract

Arctic biomes across a region including Alaska and Eastern Russia were investigated using the BIOME4 biogeochemical and biogeography vegetation model. This study investigated past (the last 21,000 years), present, and future vegetation distributions in the study area, using climate forcing from five CMIP5 models (CCSM4, GISS-E2-R, MIROC-ESM, MPI-ESM, and MRI-CGCM3). The present-day BIOME4 simulations were generally consistent with current vegetation observations in the study region characterized by evergreen and deciduous taiga and shrub tundras.

Paleoclimatological simulations were compared with pollen data samples collected in the study region. Pre-industrial biome simulations are generally similar to the modern reconstruction but differ by having more shrub tundra in both Russia and Alaska to the north, as well as less deciduous taiga in Alaska. Pre-industrial simulations were in good agreement with the pollen data. Mid-Holocene simulations place shrub tundras along the Arctic coast, and in some cases along the eastern coast of Russia. Simulations for the Mid-Holocene are in good agreement with pollen-based distributions of biomes. Simulations for the Last Glacial Maximum (LGM) show that the Bering Land Bridge was covered almost entirely by cushion forb, lichen and moss tundra, shrub tundra, and graminoid tundra. Three out of the five models' climate data produce evergreen and deciduous taiga in what is now southwestern Alaska, however the pollen data does not support this. The distributions of cushion forb, lichen, and moss tundra and graminoid tundra differ noticeably between models, while shrub tundra distributions are generally similar.

Future simulations of BIOME4 based on the RCP8.5 climate scenario indicate a northward shift of the treeline and a significant areal decrease of shrub tundra and graminoid tundra regions in the 21st century. Intrusions of cool mixed, deciduous, and conifer forests above 60°N, especially in southwest Alaska, were notable. Across eastern Russia, deciduous taiga begins to overtake evergreen taiga, except along the coastal regions where evergreen taiga remains the favored biome.

Table of Contents

	Page
Signature Page.....	i
Title Page.....	iii
Abstract.....	v
Table of Contents.....	vii
List of Figures.....	ix
List of Tables.....	xi
Acknowledgements.....	xii
Chapter 1 Introduction.....	1
1.1 Climate-Vegetation-Permafrost Interaction.....	1
1.2 Arctic Climate.....	3
1.3 Past Climate.....	4
1.3.1 Climate of the Pre-Industrial Era.....	4
1.3.2 Climate of the Mid-Holocene.....	5
1.3.3 Climate of the Last Glacial Maximum.....	6
1.4 Future Climate.....	7
1.5 Purpose of this Study.....	7
Chapter 2 Methods.....	9
2.1 Study Region.....	9
2.2 Modern Baseline Climatology.....	12
2.3 CMIP5/PMIP3 Climate Data and Time Periods.....	15
2.4 BIOME4 Model.....	16
2.5 Plant Functional Types and Biomes.....	16
2.6 Preparation of Climate Data.....	18
2.7 Validation and Pollen Mapping.....	19
2.8 Sensitivity Analysis.....	20
Chapter 3 Results.....	21
3.1 Modern Biome Reconstruction.....	21
3.2 Pre-industrial Biome Simulations.....	26

	Page
3.3 Mid-Holocene Biome Simulations.....	30
3.4 Last Glacial Maximum Biome Simulations.....	36
3.5 Future Biome Simulations.....	40
3.6 Sensitivity Analysis.....	45
Chapter 4 Summary and Conclusions.....	49
Chapter 5 References.....	51

List of Figures

	Page
Figure 1.1 Circumpolar Active Layer Permafrost System.....	3
Figure 1.2 Timing of the retreat of the North American ice sheet.....	6
Figure 2.1 The study region for this project.....	10
Figure 2.2a Simulated land area for the Last Glacial Maximum.....	11
Figure 2.2b Modern, mid-Holocene, pre-industrial, and RCP 8.5 land area.....	11
Figure 2.3 Modern climatology of seasonal air temperatures.....	13
Figure 2.4 Modern seasonal precipitation climatology.....	15
Figure 2.5 Bioclimatic limits for high-latitude biomes.....	17
Figure 3.1 Modern biome reconstruction from BIOME4.....	22
Figure 3.2 Modern day biome equivalents in Alaska.....	23
Figure 3.3 Circumpolar Arctic Vegetation Map.....	24
Figure 3.4 Modern treeline in far eastern Russia.....	24
Figure 3.5 Percent of land area coverage of simulated biomes.....	25
Figure 3.6 Pre-industrial average summer (June, July, August) seasonal monthly temperature anomalies.....	26
Figure 3.7 Growing degree days above 0°C for the pre-industrial.....	27
Figure 3.8a Pre-industrial summarized biome distribution map.....	28
Figure 3.8b Pollen sample map for 0ka.....	28
Figure 3.9 Comparison of BIOME4 pre-industrial simulations.....	29
Figure 3.10 Percent of land area coverage of simulated biomes for the pre-industrial....	30
Figure 3.11 Mid-Holocene average seasonal summer (June, July, August) monthly temperature anomalies.....	31
Figure 3.12 Growing degree days above 0°C for the mid-Holocene.....	32
Figure 3.13a Mid-Holocene summarized biome distribution map.....	33
Figure 3.13b Pollen sample map for 6ka.....	33
Figure 3.14 Comparison of BIOME4 mid-Holocene simulations.....	34
Figure 3.15 Percent of land area coverage of simulated biomes for the mid-Holocene...35	
Figure 3.17 Last Glacial Maximum average seasonal summer (June, July, August)	

monthly temperature anomalies.....	36
Figure 3.18 Growing degree days above 0°C for the Last Glacial Maximum.....	37
Figure 3.19a Last Glacial Maximum summarized biome distribution map.....	38
Figure 3.19b Pollen sample map for 21ka.....	38
Figure 3.20 Comparison of BIOME4 Last Glacial Maximum simulations.....	39
Figure 3.21 Percent of land area coverage of simulated biomes for the Last Glacial Maximum.....	40
Figure 3.22 RCP 8.5 average seasonal summer monthly temperature anomalies.....	41
Figure 3.23 Growing degree days above 0°C for the RCP 8.5 climate projections.....	41
Figure 3.24 RCP 8.5 summarized biome distribution map.....	42
Figure 3.25 Comparison of BIOME4 RCP 8.5 projections.....	44
Figure 3.26 Percent of land area coverage for RCP 8.5 climate projections.....	45
Figure 3.27 Simulated Arctic biome sensitivity to temperature changes.....	47
Figure 3.28 Simulated Arctic biome sensitivity to precipitation changes.....	48

List of Tables

	Page
Table 2.1 Simulation lengths and horizontal resolutions.....	15
Table 2.2 Circumpolar tundra biome classification.....	18

Acknowledgements

I would like to thank Drs. Kazuyuki Saito and John Walsh for guiding my first steps in scientific research as co-chairs on my committee, and for the opportunities they provided for advancement in my education and future. Thank you to committee members Dr. Nancy Bigelow for her expertise and enthusiasm, and Dr. Uma Bhatt for the absurd yet unwavering amount of support and patience she provided. I would also like to thank Drs. Donald “Skip” Walker and Dan Mann for their intriguing teaching and discussion, and Dr. Jed Kaplan for his expertise and willingness to help.

This research was funded by the National Science Foundation (ARC-1107524) and made possible by the International Arctic Research Center at the University of Alaska Fairbanks.

I would have been lost without the efforts and support from Barbara Day, James Long, Travis Brinzow, and Flora Grabowska, all of whom made me feel less incompetent about my paperwork, computer literacy, and library searching capabilities. I greatly appreciate Dr. Bette Otto-Bliesner for hosting me at NCAR, and the insightful discussions shared Dr. Samuel Levis at NCAR and Drs. Mark Serreze and Kevin Schaefer at NSIDC.

This adventure would have been full of despair and ~734% more tears if it had not been for the friends I was fortunate enough to make these last four years. Shout out to the ATM Krew – Josh Walston, Cece Borries-Strigle, Alexander Semenov, Michael Madden and Michael Pirhalla aka “The Mikes”, Mary Butwin, and Reynir Winnan. Katia Kontar and Molly Tedesche kept it real with laughter, wine, distasteful conversations, and encouragement. Much love and thanks to those who gave me life outside of school: Ellen Parker and Alaina Ctibor for engaging in my wild antics of scholastic rebellion but also acting as the voice of reason and being there for me always, and Matt and Matt aka “The Matts” for facilitating most of said rebellion. Cheers to the fine Fairbanks establishments of HooDoo Brewing, The UAF Pub, and The Marlin for hosting innumerable good times and celebrations.

I would like to thank my parents Jason and Yukari Hendricks for all their support and encouragement these last four years, and my bro Alex Hendricks for acting like my

brother even though we're biologically related. Lastly, to my dog Solstice, thank you for forcing me to exercise and for what I'm assuming were words of encouragement – woof!

1. Introduction

The Arctic is a complex system governed by interactions between individual components including the atmosphere, terrestrial ecosystem, cryosphere, and ocean. Arctic vegetation is an integral part of the Arctic system that is controlled by temperature and length of growing season (Circumpolar Arctic Vegetation Map [CAVM], 2003). “Climate and other environmental controls, such as landscape, topography, soil chemistry, soil moisture, and the available plants that historically colonized an area, also influence the distribution of plant communities” (CAVM, 2003). Arctic regions are warming at rates nearly double the global average (Intergovernmental Panel on Climate Change [IPCC], 2013). As these climate controls on vegetation are projected to change in the future via increases in greenhouse gases and subsequent warming (IPCC, 2013), it is important to understand how Arctic vegetation will be impacted by the changing climate. The vegetation-permafrost subsystem includes and interacts with the overlying climate, snow, soil, microbial activities, and permafrost. The motivation behind this modeling study is to understand how Arctic vegetation distributions could potentially change with a changing climate. I do this by examining past climates and simulating their vegetation distributions, while also looking ahead to future changes.

1.1 Climate-Vegetation-Permafrost Interaction

The relationship between climate, vegetation, and permafrost has been studied and quantified through numerous field experiments in the Arctic and Antarctic. Permafrost, which is defined as ground that is subject to temperatures at or below freezing for at least two consecutive years (van Everdingen, 2005), is driven by surface conditions. Figure 1.1 illustrates the present-day distribution of permafrost across the Arctic. “Land cover and, above all, vegetation changes are among the more important factors able to modify permafrost distribution and its thermal regime” (Cannonne et al., 2006). The layer of ground reaching from the surface to permafrost table that thaws and freezes each year is called the active layer. It had been found that the type of vegetation alters ground surface

temperatures and in turn affects active layer thickness in the Arctic (Walker et al., 2003), as well as in Antarctica (Cannonne et al., 2006). The difference in active layer thickness between two sites with similar climate was as much as 160 cm, with greater thickness (deeper seasonal thaw) occurring at a tussock grass site compared to a moss site (Cannonne et al., 2006). A study conducted in Alaska by Walker et al. (2003) examined the relationship between vegetation, soil, and thaw depth. One principle finding was that “warmer air temperatures promote deeper thaw, but the insulation provided by more dense plant canopies and thicker soil organic horizons counter this trend”. This suggests that as vegetation shifts northward, the subsequent thickening of the organic layer at a given point may help to maintain the permafrost layer. The type of permafrost can also determine how permafrost will react to changes in vegetation. Shur and Jorgenson (2007) postulated a “permafrost classification system to describe the complex interaction of climatic and ecological processes in permafrost formation and degradation”. Their system includes the five categories: (1) climate-driven; (2) climate-driven, ecosystem-modified; (3) climate-driven, ecosystem-protected; (4) ecosystem-driven; (5) ecosystem-protected. How permafrost reacts to changes in climate is based on the zone (continuous, discontinuous, sporadic) in which the permafrost is found. For example, climate-driven permafrost “can survive under warmer climatic conditions of the discontinuous permafrost zone as long as it remains protected by ecosystem properties” (Shur and Jorgenson, 2007). Other factors that impact permafrost can include elevation, slope, aspect, snow cover, bodies of water, and infrastructure (National Snow and Ice Data Center (NSIDC), accessed 2015). These and many other studies have shown the immensely complicated nature of the vegetation-permafrost subsystem.



Figure 1.1 Circumpolar Active Layer Permafrost System delineating the types of permafrost – isolated, sporadic, discontinuous, and continuous. The approximate investigation region for this study is outlined in red. (Rekacewicz, 1998).

1.2 Arctic Climate

The Arctic climate is characterized by large spatial variability and extreme annual temperature ranges, which is controlled by incoming solar radiation over the year (Arctic Climate Impact Assessment (ACIA), 2005). Due to the curvature of the earth, the intensity of the sunlight reaching the surface in the Arctic is low compared to lower latitudes, even with the long daytime of summer. Following the Laws of Thermodynamics, the surplus of solar energy received in the equatorial regions is transferred to the Arctic where energy is lost, creating an energy deficit. This puts the

Arctic in a “low thermal energy state” (Serreze and Barry, 2014). Cooler air is capable of holding less water than warmer air and which is why precipitation in the Arctic is generally low across the region (NSIDC, accessed 2015) and depends on location. For example, the Alaskan panhandle receives enough precipitation to facilitate a temperate rainforest due to its proximity to the ocean, while high Arctic regions are considered a polar desert due to the cold temperatures and lack of precipitation (Bieniek et al., 2012).

1.3 Past Climate

Over the Late Quaternary period, or more specifically the latter part of the Late Pleistocene (126 thousand years ago to 11.7 thousand years ago) and Holocene (11.7 thousand years ago to present day), the earth has experienced a number of changes in climate. These climate changes influenced the vegetation distributions, and, consequently, permafrost distributions. Much of the permafrost present today formed through the Late Pleistocene glacial period until the Last Glacial Maximum (LGM) around 21 thousand years ago (ka), and persisted through deglaciation periods such as the mid-Holocene approximately 6 ka (IPA, accessed 2015). Scientists have been able to reconstruct these past climates using proxies, such as pollen and plant macro-fossils, tree rings, ice cores, as well as employ models to understand the processes at work in the climate-vegetation-permafrost system.

1.3.1 Climate of the Pre-Industrial Era

The pre-industrial era was a period of slightly cooler temperatures than present day, with lower carbon dioxide values near 280 ppm (IPCC, 2007). The year 1850 CE, commonly used as the time of the Pre-Industrial era, is at the end of a long cooling period that lasted approximately from 1400 – 1900 CE and is also known as the Little Ice Age (LIA) (Ruddiman, 2008; Kaufman et al., 2009). This time period is used as a baseline for the impacts that humans have had on climate. There are a number of theories as to why

the climate was cooler during the LIA that include orbital forcing, switches in millennial climate oscillations, solar variability, and volcanic eruptions (Ruddiman, 2008). Pollen records show the same biomes were present in nearly the same distributions compared to modern observed vegetation distributions (Bigelow et al., 2003).

1.3.2 Climate of the Mid-Holocene

The mid-Holocene was a period of deglaciation that occurred after the LGM. Increased solar insolation during the summer in the northern hemisphere led to melting of the ice sheets (Ruddiman, 2008). This in turn led to rising sea levels creating the coastlines that are more or less similar to those of the present day. Carbon dioxide values increased to approximately 280 ppm (Ruddiman, 2008). While the entire northern hemisphere experienced a warming during the Holocene, the timing was not consistent across the region. In fact, northwest North America, including the study region, experienced warming between 11 and 9 ka, while northeast Canada experienced warming approximately 4000 years later due to the lingering effects of the Laurentide Ice Sheet (Figure 1.2; Kaufman, 2004). Local summer temperatures were on average $1.6^{\circ}\text{C}\pm 0.8^{\circ}\text{C}$ warmer than present in the western Arctic (Kaufman et al., 2004), or more than 5°C warmer than preindustrial temperatures at high latitudes with June being the warmest month in northern Russia and northwest North America (Renssen et al., 2012). While warming was significant during the mid-Holocene, the treeline, or tree-tundra boundary, was not north of its present position the study region (Bigelow et al., 2003). Based on pollen records, much of the vegetation found across the region today was present and in relatively the same distribution during the mid-Holocene (Bigelow et al., 2003).

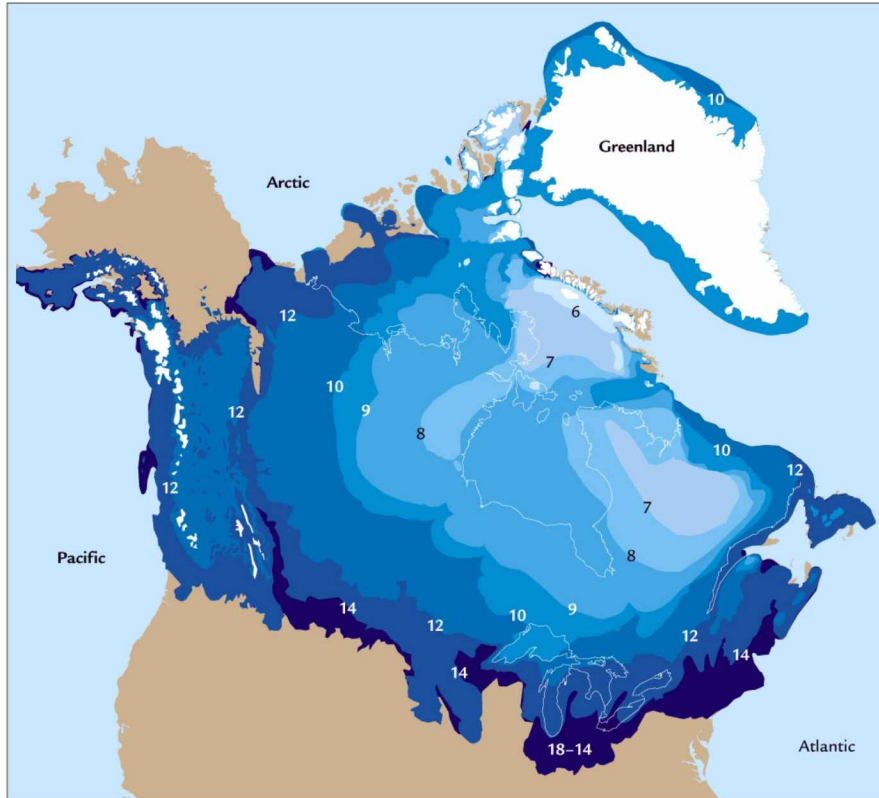


Figure 1.2 Timing of the retreat of the North American ice sheet during the transition from LGM to Holocene. Contours and numbers represent radiocarbon dating of the ice edge in thousands of years before present from remains along the edge of the ice sheet, showing non-uniform retreat of the ice sheet (Ruddiman, 2008).

1.3.3 Climate of the Last Glacial Maximum

The Last Glacial Maximum was colder, windier, and drier than the present day (Ruddiman, 2008; Hopkins et al., 1982). The solar insolation levels were nearly the same values as today, however, the large expanses of land ice and low carbon dioxide values (~185 parts per million) may be the reason why the LGM was so cold, dry, and windy (Ruddiman, 2008). During this time period, sea levels were approximately 125 m lower than modern levels due to freshwater storage in the land ice (Ruddiman, 2008). This lowered sea level exposed the land bridge that connected what is now Russia and Alaska, also known as the Bering Land Bridge. During the LGM, the Land Bridge was covered in

dry Arctic grass (graminoid) tundra and sparse shrub tundra, according to pollen records (Bigelow et al., 2003).

1.4 Future Climate

Based on numerous climate simulations, the climate is projected to warm in the future due to increasing radiative forcing caused by increased greenhouse gases (IPCC, 2013). The IPCC has constructed future climate scenarios based on greenhouse gas emissions and their consequent radiative forcing (in W/m^2) on the earth. Of the four Representative Concentration Pathways (RCP), we are tracking closest to RCP 8.5. This means that if we continue emitting greenhouse gases without any mitigation or reduction efforts, we can expect to see an increase in radiative forcing by 8.5 W/m^2 . With this increase in radiative forcing, some projections are showing global temperatures increasing by $3.7^\circ\text{C} \pm 1.1^\circ\text{C}$ by the end of this century, with more rapid warming in the Arctic (IPCC, 2013). Carbon dioxide values are projected to be 936 ppm by the year 2100 CE (IPCC, 2013).

1.5 Purpose of this Study

Over the course of this project, I aimed to answer three major questions:

1. How well is Arctic vegetation simulated during the Late Quaternary period under different climate conditions?
2. How sensitive are simulated biomes to changes in climate?
3. What are the future projections of Arctic vegetation under the IPCC RCP 8.5 climate scenario and what are the consequent impacts?

While the sensitivities explained in (2) and (3) are based on one-way interactions between climate and vegetation (climate driving vegetation), the sensitivities have important implications for feedbacks to high-latitude climate. These feedbacks are beyond the scope of the presented study, which can nevertheless be viewed as a first step toward and assessment of the strength of terrestrial feedbacks in which vegetation plays a role.

2. Methods

My research was conducted by running BIOME4 (Kaplan et al., 2003), a global equilibrium biogeochemistry-biogeography model, to produce biome distributions in the Arctic. The focus was on Beringia, which includes far eastern Russia, Alaska, and Canada west of the Mackenzie River.

2.1 Study Region

The study region focused on the area bounded by a southern limit at 50°N, northern limit at 80°N, eastern limit at 150°E, and western limit at 120°W (Figure 2.1). I chose these boundaries to make the results comparable with previous research that was used as a guide for this project (Kaplan et al., 2003; Bigelow et al., 2003). This region has experienced changes in climate, geography, and vegetation over the last 21,000 years, which makes understanding the processes in this region important for climate scientists.

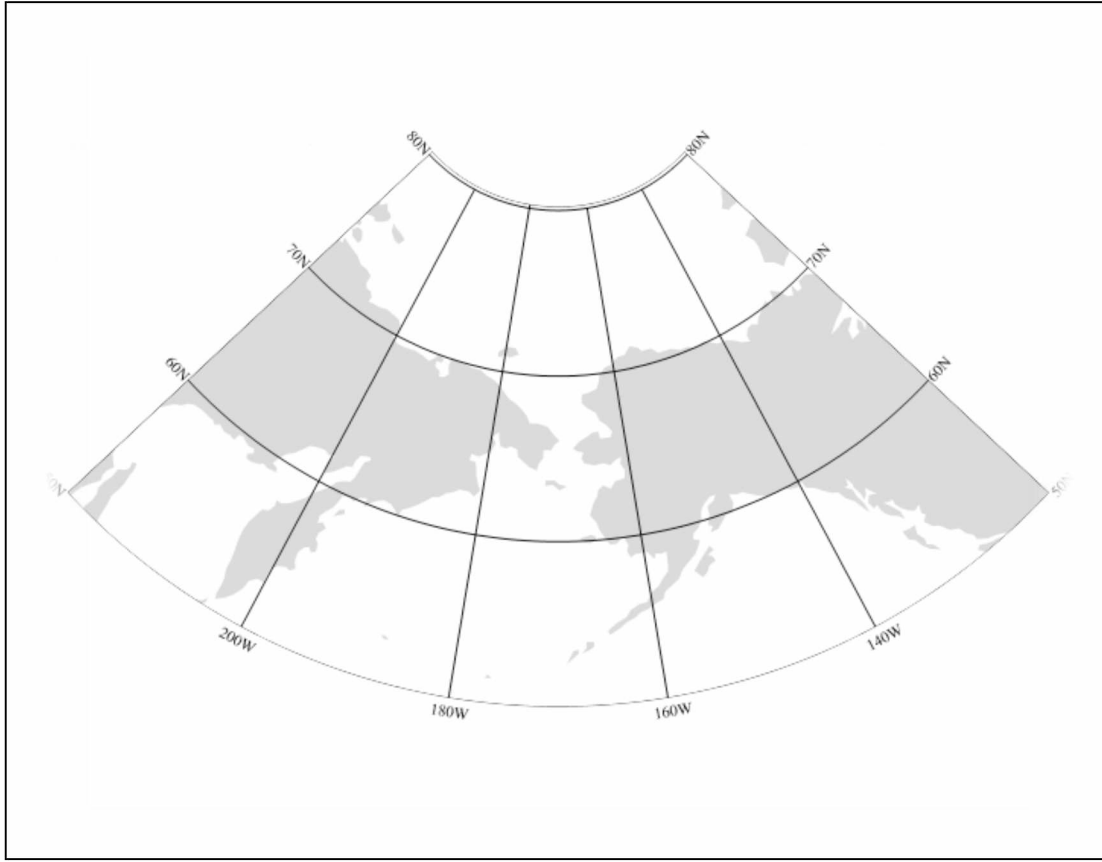


Figure 2.1 The study region for this project is an area enclosed by 50°N – 80°N, 150°E – 120°W and includes what is now eastern Russia and Alaska.

For all of the simulations, the coastlines were determined by grid cells with greater than fifty percent land area at a $0.5^\circ \times 0.5^\circ$ resolution (Figure 2.2). This method produced coastlines that are obviously rougher than actual coastlines; however, the modeled coastlines approximated the land region reasonably well at the prescribed resolution.

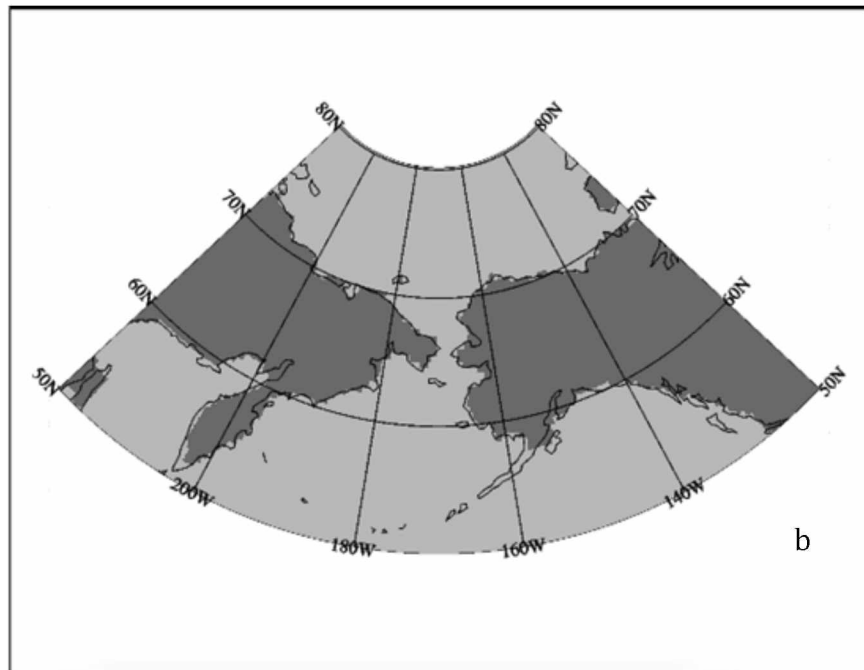
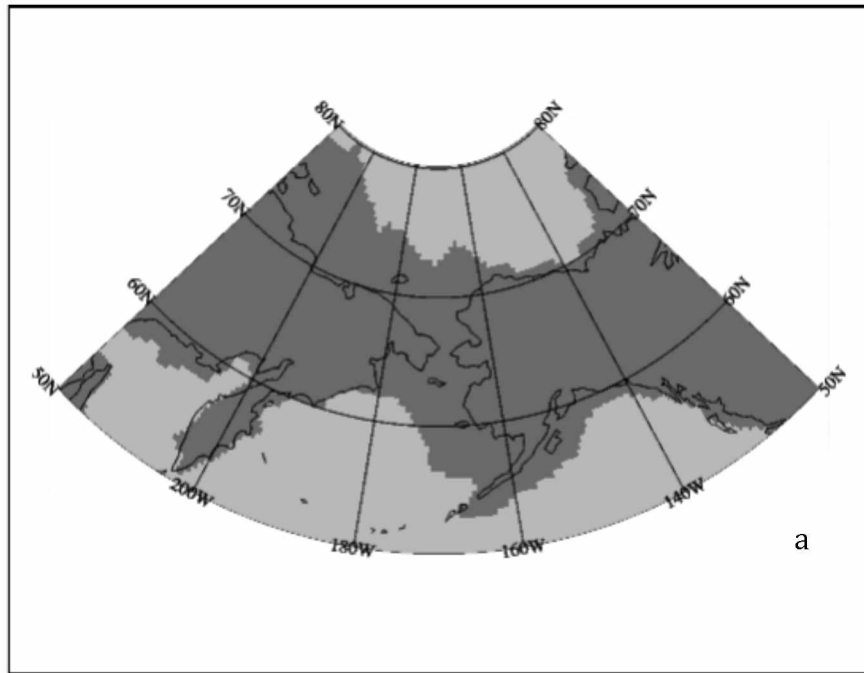


Figure 2.2 a.) Simulated land area for the Last Glacial Maximum; b.) Modern, mid-Holocene, pre-industrial, and RCP 8.5 land area

2.2 Modern Baseline Climatology

The baseline modern climatology was compiled from the University of Delaware temperature and precipitation data (Matsuura and Willmott, 2009a, 2009b) and European Center for Medium-range Weather Forecasts's (ECMWF) ECMWF Reanalysis-40 (ERA-40) sunshine data (Uppala et al., 2005). Long-term monthly mean values of temperature and precipitation (version 2.01) were compiled from global station data (Matsuura and Willmott, 2009a, 2009b). The temperature and precipitation climate data was available at a $0.5^{\circ}\times 0.5^{\circ}$ resolution (Figures 2.3 and 2.4). Monthly means of daily values of sunshine data from ECMWF's ERA-40 (1957-2002), originally at a $2.5^{\circ}\times 2.5^{\circ}$ resolution, were interpolated to $0.5^{\circ}\times 0.5^{\circ}$ resolution. Modern simulations were conducted using climate data from the years of approximately 1959 – 2000.

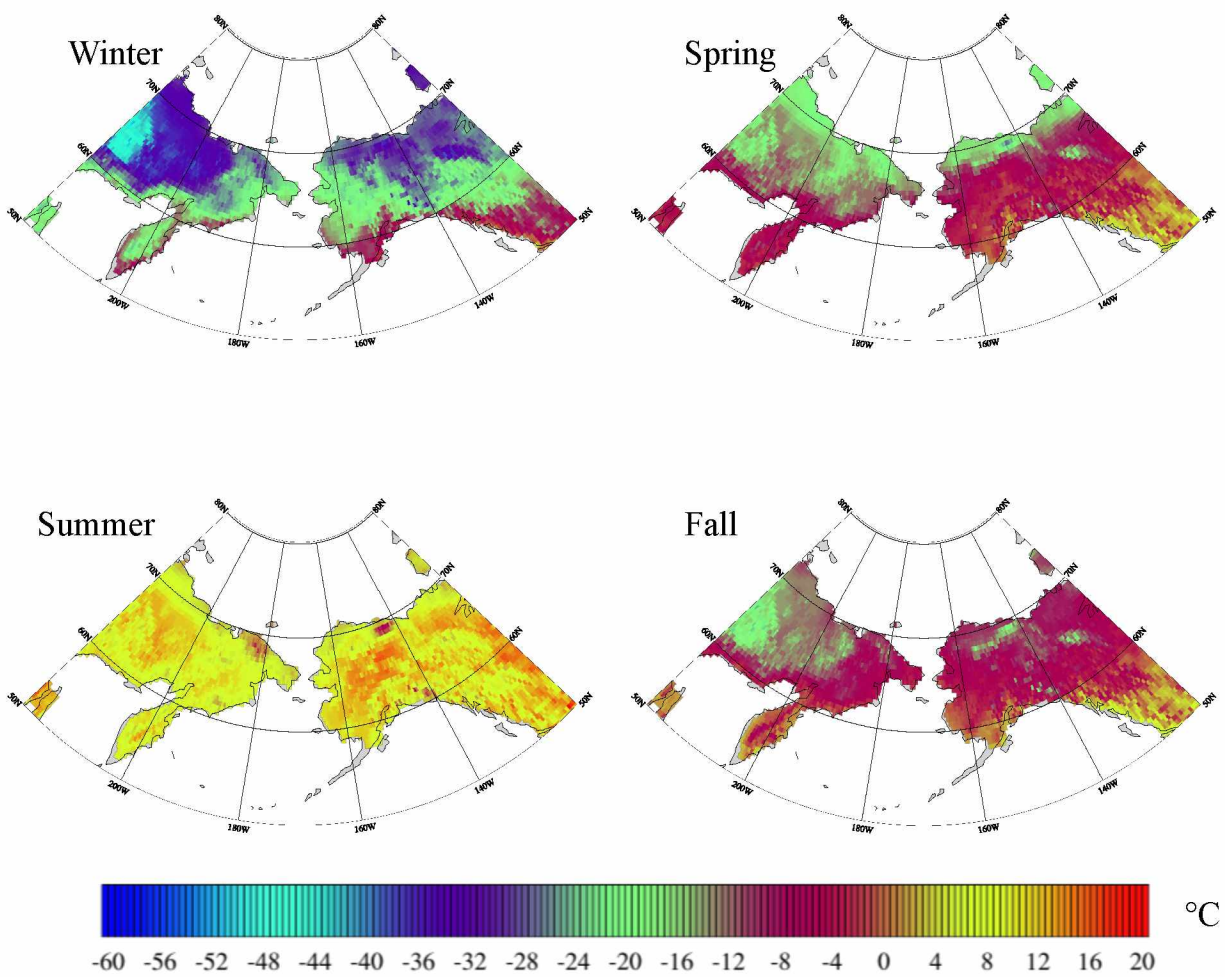


Figure 2.3 Modern climatology of seasonal air temperatures based on University of Delaware climate data (Matsuura and Willmott, 2009a). Months for each season are: winter = December, January, February; spring = March, April, May; summer = June, July, August; fall = September, October, November.

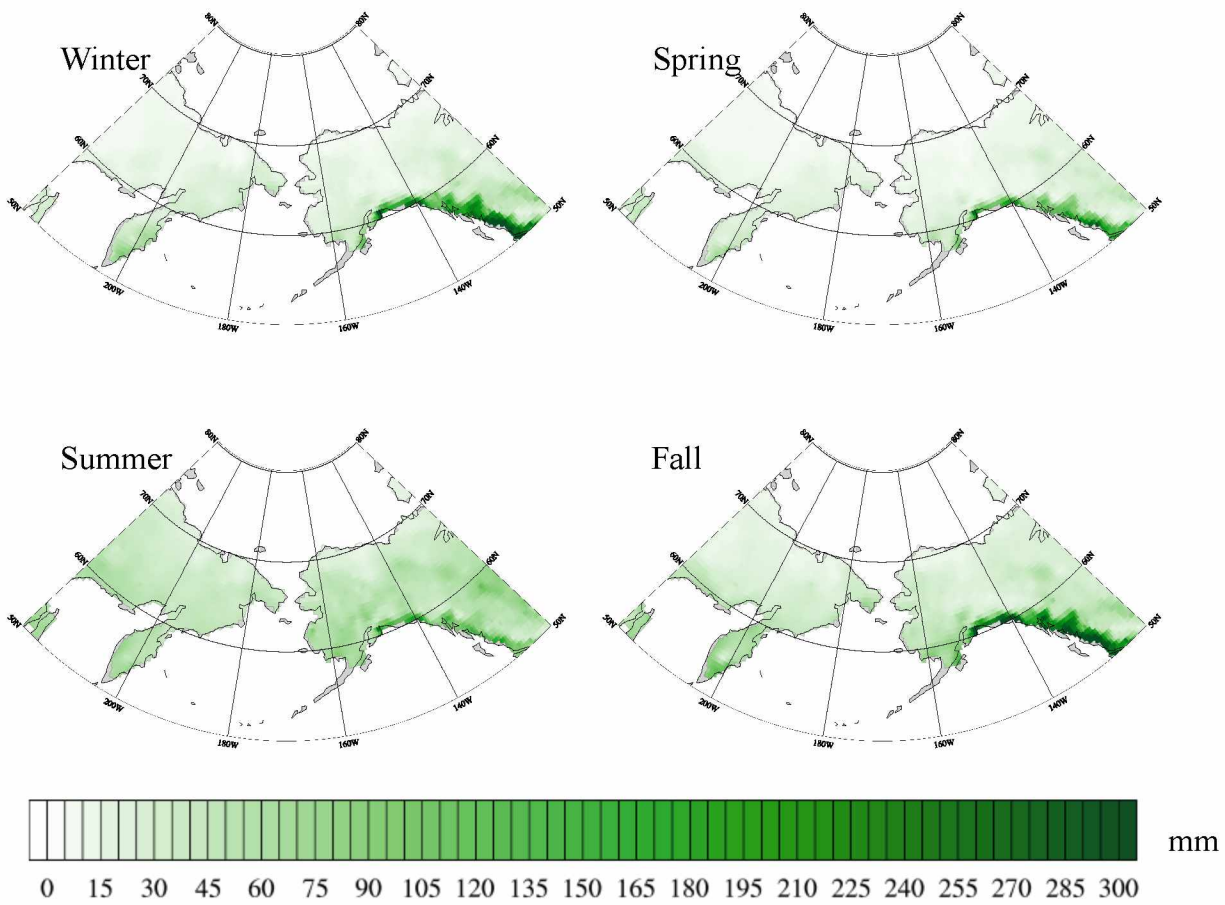


Figure 2.4 Modern seasonal precipitation climatology based on the University of Delaware climate data. (Matsuura and Willmott, 2009b). Months for each season are: winter - December, January, February; spring - March, April, May; summer - June, July, August; fall - September, October, November.

2.3 CMIP5/PMIP3 Climate Data and Time Periods

Modeled climate data from the Coupled Model Intercomparison Project Phase 5 (CMIP5, Taylor et al., 2012) and Paleoclimate Modeling Intercomparison Project Phase 3 (PMIP3, Braconnot et al., 2012) was obtained through the Earth System Grid Federation portal (Table 2.1). All GCM data were interpolated to $0.5^{\circ} \times 0.5^{\circ}$ globally. The models used in this project were chosen based on the climate variables available for each of the four time slices so that the same variables from each model can be used for consistency. These models are: CCSM4 (Gent et al., 2011); GISS-E2-R (Schmidt et al., 2014); MIROC-ESM (Watanabe et al., 2011); MPI-ESM (Brovkin et al., 2013); MRI-CCSM3 (Yukimoto et al., 2012). The variables used are surface air temperature, precipitation flux at the surface, surface downwelling shortwave radiation, and surface downwelling clear-sky shortwave radiation.

Table 2.1 Simulation lengths and horizontal resolutions (degrees latitude \times degrees longitude) for CMIP5/PMIP3 climate data.

	CCSM4 1.06° \times 1.25°	GISS-E2-R 2° \times 2.5°	MIROC-ESM 2.8125° \times 2.8125°	MPI-ESM 1.875° \times 1.875°	MRI-CGCM3 1.125° \times 1.125°
LGM	101 years	25 years	100 years	100 years	100 years
Mid-Holocene	301 years	25 years	100 years	100 years	100 years
Pre-industrial	251 years	25 years	99 years	200 years	500 years
Future RCP 8.5	2006-2100	2006-2025	2006-2100	2070-2100	2006-2100
Control	1979-2010	1910-1950	1979-2006	1979-2008	1979-2010
References	Gent et al., 2011	Schmidt et al., 2014	Watanabe et al., 2011	Brovkin et al., 2013	Yukimoto et al., 2012

The project focused on four distinct time periods: the Last Glacial Maximum 21,000 years ago, mid-Holocene 6,000 years ago, pre-industrial era centered at 1850 CE, and a future simulation for the 21st century. Some variables had data available for longer time periods, but for consistency we kept the majority of the future climate data within this time period. Three GCMs (CCSM4, MIROC-ESM, MRI-CGCM3) provided climate data for the entire 21st century up to 2100 and the data were averaged over the whole period. MPI-ESM climate data were for the latter part of the 21st century, from 2070 – 2100, and GISS-E2-R climate data were for the early part of the 21st century, from 2006 – 2025. These differences in timing of GCM climate data

provide insight into how the equilibrium biome distribution might look in the early, late, and average climate simulations for the 21st century. However, the use of different time periods precludes a systematic comparison of the across-model changes, as the late-century forcing is considerably stronger than the early-century forcing in the RCP 8.5 scenario

2.4 BIOME4 Model

BIOME4 simulates steady state biome distributions under given climate conditions. The simulations are run on a $0.5^{\circ} \times 0.5^{\circ}$ latitude/longitude grid for the whole globe, after which I focused the results on the bounded study region. BIOME4 is driven by long-term mean monthly climate data and soil texture information. Compared to other vegetation models that calculate transient vegetation pattern changes or energy or nutrient fluxes, BIOME4 was ideal for this project because of the steady state vegetation computations. Permafrost reactions to changes in climate and surface changes are delayed due to insulation and thermal inertia (the heat capacity of the sub-surface), therefore, it made more sense to focus on climate “snapshots” for each of the time slices. These time slices are separated by long-term climate shifts.

The climate variables required to force BIOME4 are long-term mean monthly temperature, precipitation, and percent sunlight (see Eqs. in 2.5.2). Water holding capacity and percolation rates are calculated from the soil texture information provided by the FAO digital soil map (as used by Kaplan et al., 2003). Carbon dioxide values are prescribed at the beginning of each model run and remained constant for each time period: LGM = 185 parts per million (ppm); mid-Holocene and Pre-Industrial Era = 280 ppm; future = 936 ppm. For the modern simulation, I used 385 ppm.

2.5 Plant Functional Types and Biomes

BIOME4 uses the prescribed climate data to calculate plant functional types (PFTs). PFTs are classifications of plants based on life form, leaf morphology, phenology, and mechanism of extreme cold tolerance (Bigelow et al., 2003). After PFTs are calculated, BIOME4 ranks tree and

non-tree PFTs that were calculated within a grid cell, using variables such as net primary productivity (NPP), leaf area index (LAI), and mean annual soil moisture, which are internally calculated in BIOME4 (Kaplan et al., 2003). Based on the ranking combinations, a biome is assigned to each grid cell. “Each PFT is assigned a small number of bioclimatic limits which determine whether it could be present in a given grid cell...” (Kaplan et al., 2003). Figure 2.5 shows the bioclimatic limits that each Arctic PFT is allowed to occupy.

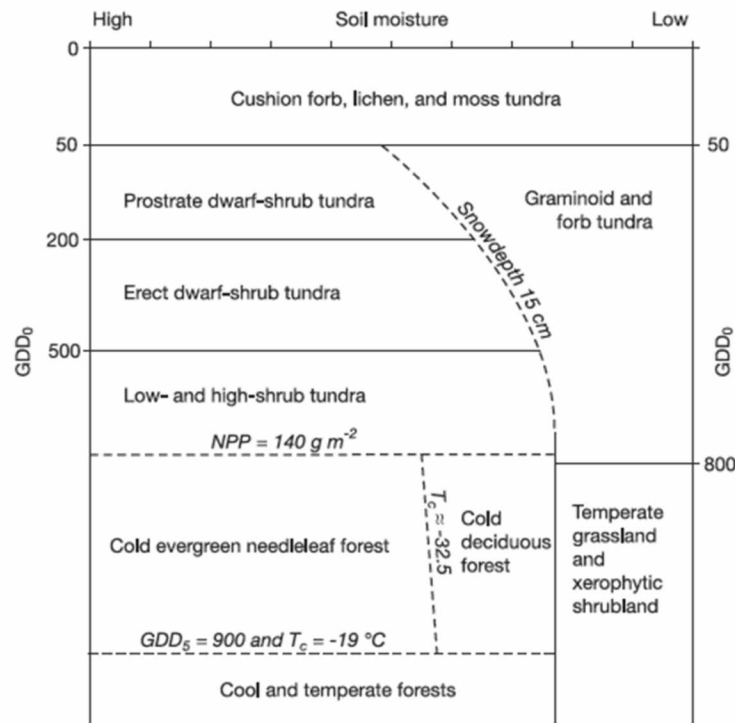


Figure 2.5 Bioclimatic limits for high-latitude biomes taken from Kaplan et al., 2003. Growing degree days above 0°C (GDD₀) is defined as the accumulated temperature for the growing season, which for the Arctic is above freezing. (GDD₅ is the growing degree days above 5°C.)

BIOME4 has a total of 27 biomes that can be assigned to a grid cell globally. BIOME4 was optimized for modern Arctic simulations and as such has five distinct tundra biomes, which were not present in the previous version BIOME3 (Haxeltine and Prentice, 1996). These tundra biomes are: cushion forb, lichen, and moss tundra; prostrate shrub tundra; dwarf shrub tundra;

shrub tundra; graminoid tundra. Definitions and examples of these tundra types can be found in Table 2.2. In addition to the tundra biomes, BIOME4 has two Arctic tree biomes, evergreen taiga (ex. *Picea glauca*, *Picea mariana*) and deciduous taiga (ex. *Betula papyrifera*, *Populus tremuloides*, *Larix laricina*). Table 2.2 from Kaplan et al., 2003, summarizes the biome classification scheme as well as provides typical species for each biome.

Table 2.2 Circumpolar tundra biome classification from Kaplan et al. (2003).

Biome	Definition	Typical Taxa
Low- and high-shrub tundra	continuous shrubland, 50 cm to 2 m tall, deciduous or evergreen, sometimes with tussock-forming graminoids and true mosses, bog mosses and lichens	<i>Alnus</i> , <i>Betula</i> , <i>Salix</i> , <i>Pinus pumila</i> (in eastern Siberia), <i>Eriophorum</i> , <i>Sphagnum</i>
Erect dwarf-shrub tundra	continuous shrubland 2–50 cm tall, deciduous or evergreen, with graminoids, true mosses and lichens	<i>Betula</i> , <i>Cassiope</i> , <i>Empetrum</i> , <i>Salix</i> , <i>Vaccinium</i> , Gramineae, Cyperaceae
Prostrate dwarf-shrub tundra	discontinuous shrubland of prostrate deciduous shrubs, 0–2 cm tall	<i>Salix</i> , <i>Dryas</i> , <i>Pedicularis</i> , Asteraceae, Caryophyllaceae, Gramineae, true mosses
Cushion forb, lichen and moss tundra	discontinuous cover of rosette plants or cushion forbs with lichens and mosses	<i>Papaver</i> , <i>Draba</i> , Saxifragaceae, Caryophyllaceae, lichens, true mosses
Graminoid and forb tundra	predominantly herbaceous vegetation dominated by forbs and graminoids, with true mosses and lichens	<i>Artemisia</i> , <i>Kobresia</i> , Brassicaceae, Asteraceae, Caryophyllaceae, Gramineae, true mosses

2.6 Preparation of Climate Data

Before I ran BIOME4 with CMIP5/PMIP3 data, I applied the delta method using the compiled baseline modern climatology. The delta method is applied to climate data to remove bias in the GCM climate data. All GCMs have some form of bias in the data inherent to the models, for example simulated temperatures can be too high or too low at specific locations. By applying the delta method, I can alleviate the local differences in biases by using the modern climatology as a baseline climate scenario. The GCM based anomalies for each time period are added to the baseline climatology and the combined data set is then used to force BIOME4 simulations. These calculations were done for each calendar month for each model and the climate forcing was constructed based on the following equations:

Temperature (K):
$$T = (T_{Model} - T_{Control}) + T_{Modern} \quad \text{Eq. 1}$$

Precipitation (mm):
$$P = \frac{P_{Model}}{P_{Control}} \times P_{Modern} \quad \text{Eq. 2}$$

Sunshine (%):
$$S = \frac{(SD_{Model} - SD_{Control}) + SD_{Modern}}{(SC_{Model} - SC_{Control}) + SC_{Modern}} \quad \text{Eq. 3}$$

where Model = CMIP5/PMIP3 climate data; Control = CMIP5/PMIP3 modern climate data; Modern = modern climatology; SD = downwelling radiation; and SC = clear sky downwelling radiation. For a complete data set, BIOME4 created 21 simulations: 4 time periods \times 5 GCM climate data, plus a single modern biome simulation using the modern climatology.

2.7 Validation and Pollen Mapping

I compared the BIOME4 simulations with pollen maps. Pollen data and maps were updated from Bigelow et al., 2003, where pollen data were converted into biomes. Pollen samples were taken from lake sediments or peat deposits and radiocarbon dated using the carbon-14 isotope, or ^{14}C . Pre-industrial and mid-Holocene pollen samples were chosen within at least 500 years of the time slice (and most samples were within 200 years). Because of the lack of LGM-aged pollen sites, LGM pollen samples date within at least 1000 years of the time slice (Bigelow et al., 2003). Due to legacy datasets (c.f. Edwards et al., 2000; Bigelow et al., 2003) that included the pollen sample closest to 6000 ^{14}C years, the mid-Holocene samples here also date to 6000 ^{14}C years. However, because of fluctuations of ^{14}C in the atmosphere, 6000 ^{14}C years is approximately 6800 calendar years, and 6000 calendar years approximates 5300 ^{14}C years. This mismatch between the mid-Holocene GCM runs (at 6000 calendar years) and the pollen data (at 6000 ^{14}C years), does not affect the pollen biomisation results. When a subset of the Beringian pollen data (63 sites) was analyzed at both 6000 calendar years and 6000 ^{14}C years, 84% of the

sites had the same biome for both the 6000 calendar year and 6000 ^{14}C year samples. By the LGM (21ka), 18k ^{14}C years is the same as 21k calibrated years. For each time period, the following numbers of sites are present to which BIOME4 simulations can be compared: 0ka = 877 sites; 6ka ^{14}C = 132 sites; and 18ka ^{14}C = 29 samples from 26 sites. For future simulations, I evaluated the output with other literature on possible vegetation distributions, mainly from Kaplan and New (2006).

2.8 Sensitivity Analysis

To understand how changing single climate variables can affect the simulated biome distributions, I conducted a series of sensitivity experiments. For the analysis, modern temperature and precipitation values were changed linearly from the long-term mean monthly climatological values within a prescribed range. Temperature was changed by 2°C increments from monthly values for a total range of $\pm 10^{\circ}\text{C}$ across all months. Precipitation was changed by multiples of 10% of mean monthly precipitation values for a total range of $\pm 150\%$ across all months.

3. Results and Discussion

The following chapter discusses the results from the BIOME4 simulations. The modern biome reconstruction will be discussed first to give a reference and comparison for the four time slices. After the modern reconstruction, I will show the pre-industrial, mid-Holocene, LGM, and future biome simulations. Each time period, not including the modern reconstruction, will present a summarized biome distribution for all five GCMs, an analysis of BIOME4 simulations compared to pollen maps, as well as similarities and differences between GCMs. A discussion of the sensitivity experiment is presented at the end of this chapter.

3.1 Modern Biome Reconstruction

The modern biome reconstruction (Figure 3.1) is generally realistic at a $0.5^{\circ} \times 0.5^{\circ}$ resolution based on a visual analysis. The majority of vegetation simulated in the study region consists of shrub tundra, dwarf shrub tundra, prostrate shrub tundra, evergreen taiga, and deciduous taiga. Small regions of cushion forb, lichen, and moss tundra, and temperate xerophytic grassland are simulated, as well as the warmer cool conifer forest, cold mixed forest, warm mixed forest, and temperate mixed forest in the southeastern portion of the study area. This is consistent with present day observed biomes (Viereck and Little, 1972) and can be seen in Figures 3.2, 3.3, and 3.4 (Boggs et al., 2014a, 2014b; CAVM, 2003; Garsia, 1990). Figure 3.2 shows the present day biomes in Alaska compiled by Boggs et al. (2014a, 2014b). Biomes were assigned to each coarse vegetation class in the original maps. As biomes are more general than the classes, several classes were grouped into a single biome. For example, the evergreen taiga biome includes four classes (where evergreen conifers dominate) that vary according to tree density (closed, open, or woodland), as well as the presence and abundance of secondary deciduous trees. Figure 3.3 shows the CAVM, which was compiled by a group of international experts on vegetation in their respective regions. This map shows the extent of the tundra, which is bounded to the south by the treeline.

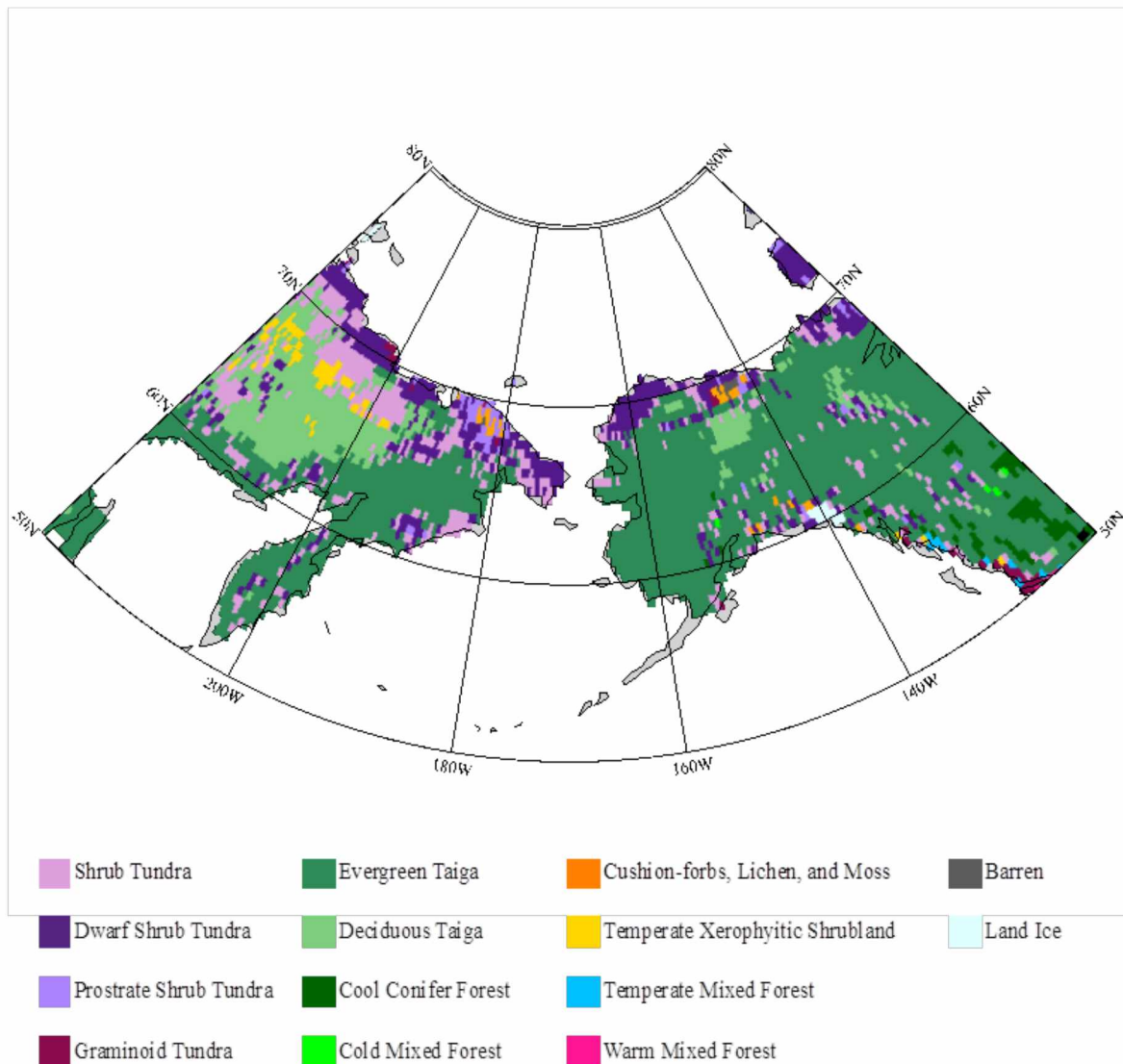


Figure 3.1 Modern biome reconstruction from BIOME4 driven by modern climatology data from the University of Delaware and ERA-40.

Although the modern biome reconstruction approximates the observed biome distributions in many areas, there are major differences from actual present day vegetation. These differences include evergreen taiga and deciduous taiga simulated north of the Brooks Range in northern Alaska and along the western portion of Alaska. Figures 3.2 and 3.3 show tundra rather than taiga exists in these regions. Kaplan et al. (2003) posits “the influence of heavy cloud cover combined with low sun angles on surface solar radiation may be responsible for the disagreement in hypermaritime regions, such as southwest Alaska”. Discrepancies in the

reconstruction north of the Brooks Range could be the result of climate data that derives from a sparse station network that was interpolated to cover a large area. These few stations would not be representative of the climate here and would simulate biomes that are not accurate at the grid cell location. BIOME4 was optimized for the Arctic regions (Kaplan et al., 2003) so it would produce more accurate simulations if more skillfully downscaled data was provided, but that was beyond the scope of this project.

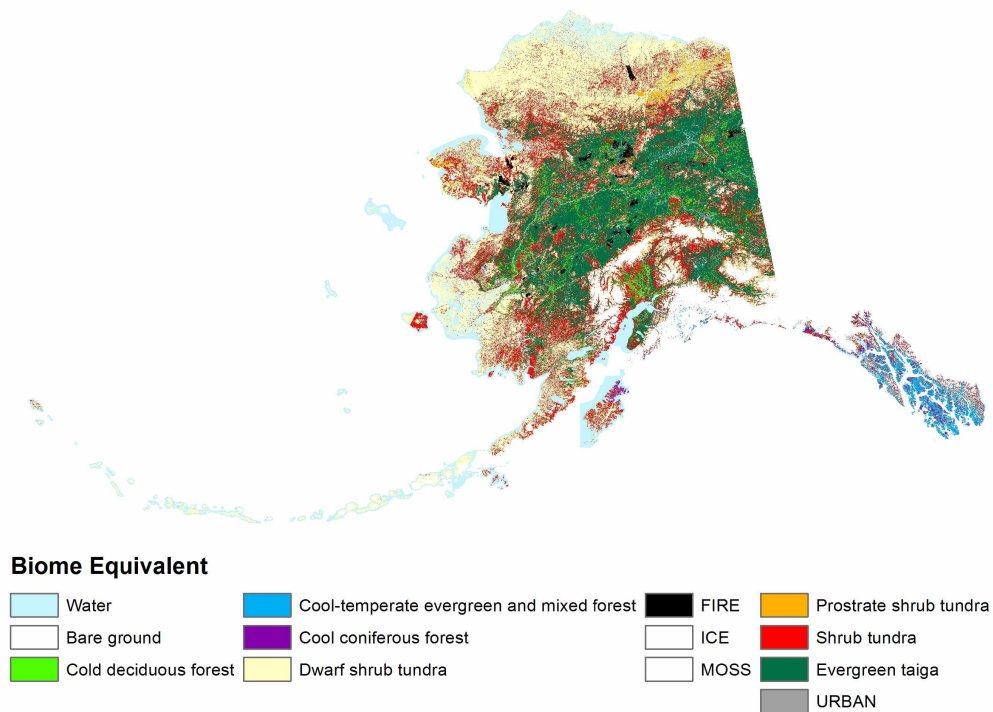


Figure 3.2 Modern day biome equivalents in Alaska (Boggs et al., 2014a, 2014b: <http://aknhp.uaa.alaska.edu>).

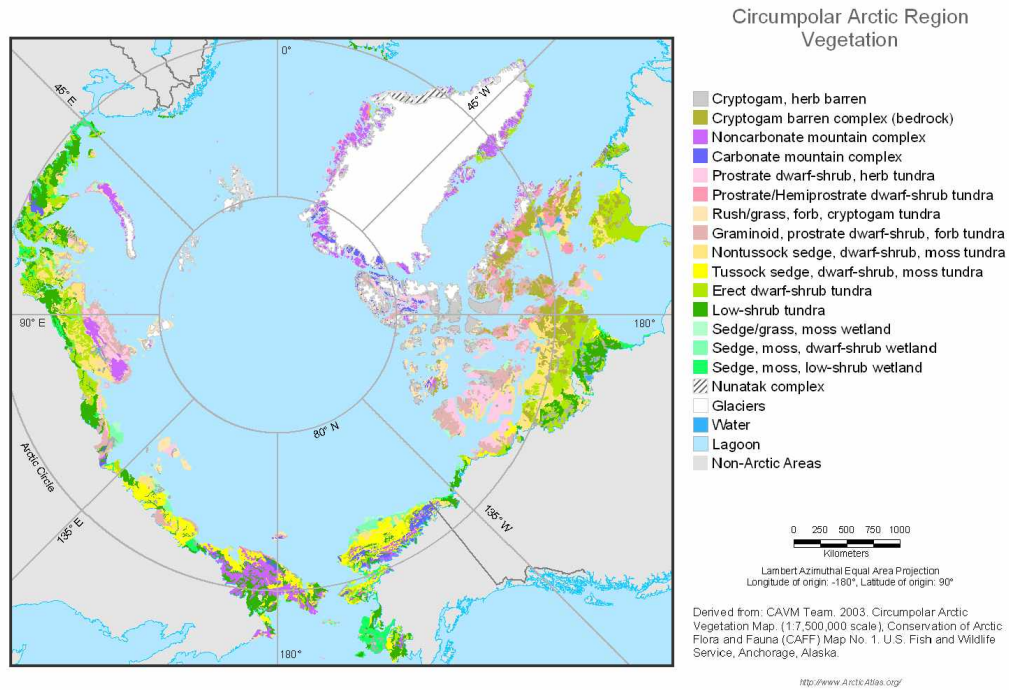


Figure 3.3 Circumpolar Arctic Vegetation Map (CAVM, 2003). This map shows the extent of the modern tundra. The southern boundary of this map is the treeline.

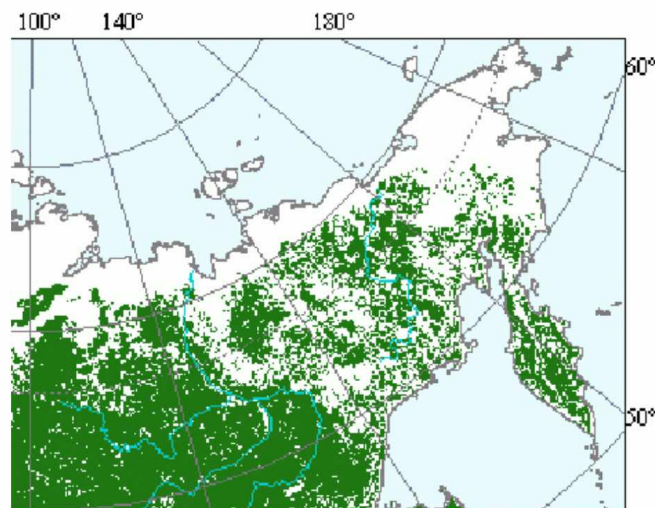


Figure 3.4 Modern treeline in far eastern Russia (adapted from Garsia, ed. 1990).

Growing season length and summer temperatures drive Arctic vegetation (CAVM, 2003). This can be seen in the modern biome reconstruction and is consistent with observed biome

gradients. Colder dwarf shrub and prostrate shrub tundra are simulated along the Arctic coast, with warmer shrub tundra bordering dwarf shrub and prostrate shrub tundra at lower latitudes and farther inland. The only region not simulated to have shrub tundra along the Arctic coast is in the Mackenzie River Delta region in Northwest Territories, where taiga is accurately simulated. Evergreen taiga in Alaska and both evergreen taiga and deciduous taiga in eastern Russia are simulated at lower latitudes and farther inland. In eastern Russia, evergreen taiga dominates the southern and eastern portions of the region, while deciduous taiga is simulated in the interior region. The simulated percent of total land area covered by these biomes are (Figure 3.5): cushion forb, lichen and moss tundra 1%; shrub tundra (includes shrub, dwarf shrub, and prostrate shrub biomes) 25%; evergreen taiga 57%; deciduous taiga 12%; cool conifer forest 2%. All other biomes including land ice make up the remaining 3% of land area.

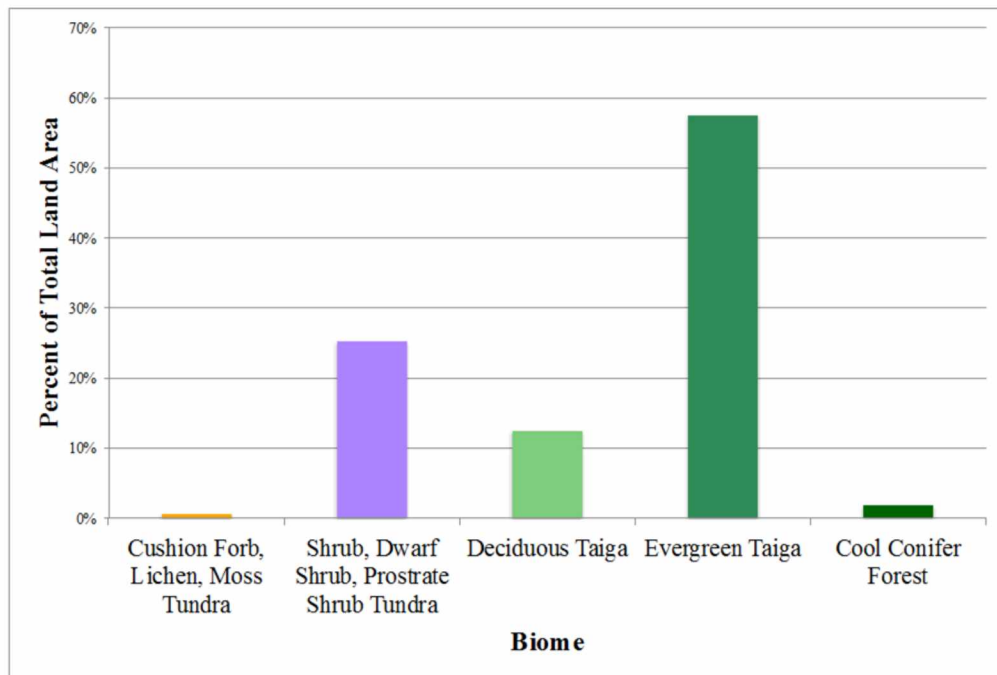


Figure 3.5 Percent of land area coverage of simulated biomes for the modern reconstruction.

3.2 Pre-Industrial Biome Simulations

Pre-industrial climate data from the chosen CMIP5/PMIP3 GCMs show generally cooler summer seasonal average temperatures (Figure 3.6). CCSM4 and MPI-ESM provided the coolest summer seasonal average temperatures while GISS-E2-R provided the warmest temperatures during the growing season. The Arctic's short growing season is limited to the summer months. Figure 3.7 shows the growing degree days above zero for the pre-industrial GCMs calculated by BIOME4. The cooler climate data is apparent in the cooler CCSM4 and MPI-ESM with lower GDD_0 index values. Higher GDD_0 index values are shown for the warmer GISS-E2-R summer temperatures which are similar to modern GDD_0 values.

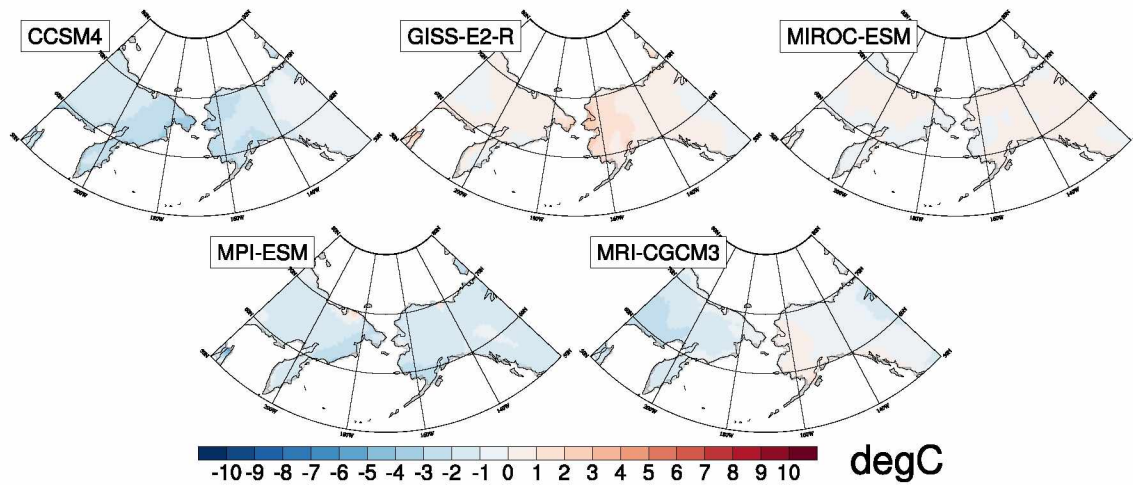


Figure 3.6 Pre-industrial average summer (June, July, August) seasonal monthly temperature anomalies from modern baseline climate.

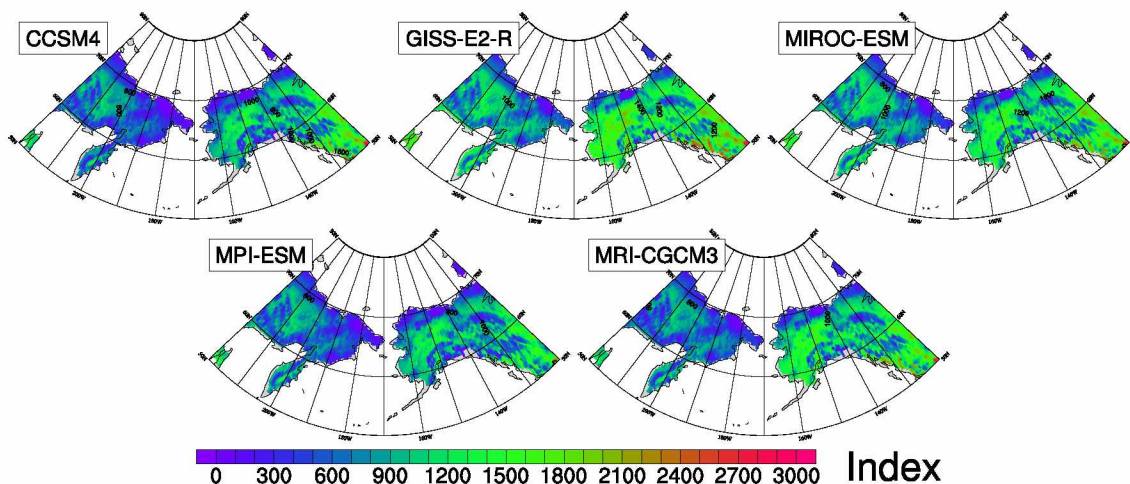


Figure 3.7 Growing degree days above 0°C for the pre-industrial time period.

The composite map of the simulated pre-industrial biomes is generally similar to the modern biome reconstruction (Figure 3.8a). At least three models out of five were required for a composite map to produce the same biome at a grid cell with color. Black cells indicate that no single biome was simulated by at least three models. This is in contrast to the gray cells that are simulated as barren. Much of the vegetation simulated for the pre-industrial is shrub tundra, dwarf shrub tundra, prostrate shrub tundra, deciduous taiga, and evergreen taiga. All of these biomes exist in the modern reconstruction. More cushion forb, lichen, and moss tundra is produced for this period compared to the modern reconstruction. The pre-industrial simulation places the treeline in Russia south of its modern reconstruction as well as simulates more tundra. Alaska's biome distribution remains largely the same with evergreen taiga covering most of the state along the same treeline when compared to modern reconstruction. The Brooks Range and western Alaska is simulated as taiga, however, this region should ideally be simulated as shrub type tundras. Since this map is generated by a majority rule, it is interesting to point out that the majority of models were in agreement for the same problem areas. The summarized biome distribution maps were created using a majority rule at each grid cell.

From the Oka pollen map (Figure 3.8b), it appears that BIOME4 simulates the pre-industrial biome distribution fairly well. The pre-industrial era has a large pollen sample network in Alaska, which makes a comparison between simulations and actual vegetation straightforward. The pollen map clearly displays Alaska's tundra and taiga boundary with

Interior Alaska largely dominated by evergreen taiga, while northern and western Alaska are covered in shrub type tundras. This is in contrast to BIOME4 simulations that place evergreen taiga across nearly the entire western portion of Alaska and north of the Brooks Range. The pollen sample network in Russia has fewer sample locations but a comparison between the simulation and pollen map is still possible. Pollen samples in Russia show the northern and northeastern coasts dominated by shrub tundras while the interior is dominated by shrub tundras and deciduous taiga. A notable discrepancy in Russia is the simulation of evergreen taiga along the southern region of Russia where the few pollen samples indicate deciduous taiga. The pollen map also shows warmer biomes than were simulated in southern and southeastern Alaska.

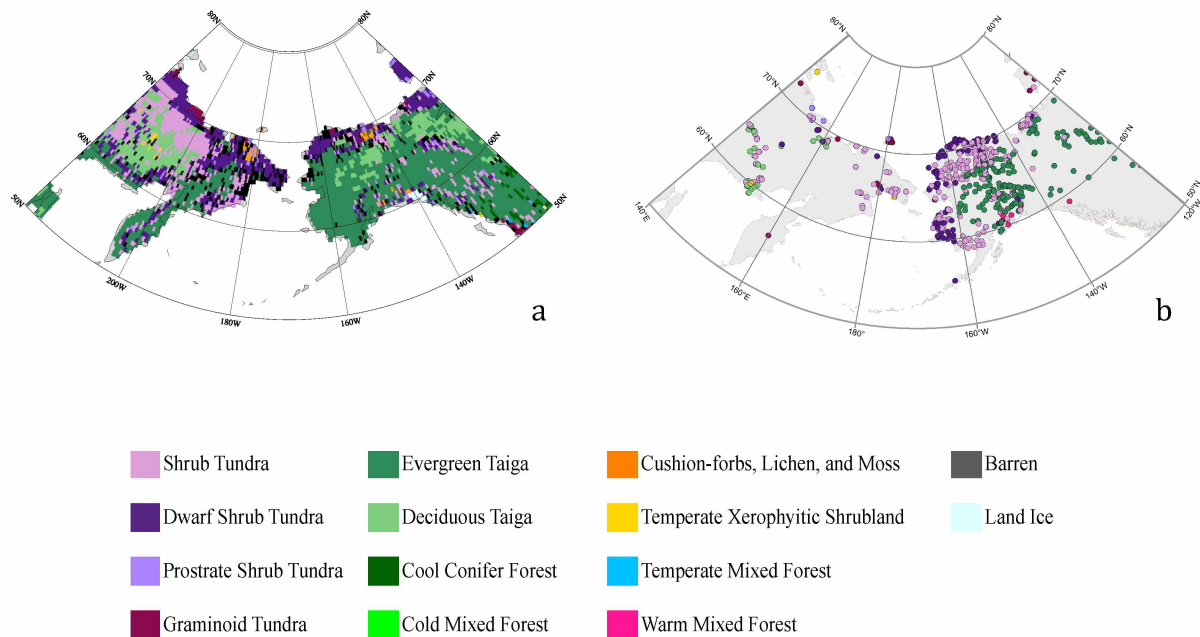


Figure 3.8 a.) Pre-industrial summarized biome distribution map for all five CMIP5/PMIP3 GCMs; b.) pollen sample map for 0ka. At least three models out of five were required for a composite map to produce the same biome at a grid cell with color. Black cells indicate that no single biome was simulated by at least three models.

CMIP5/PMIP3 pre-industrial climate varies slightly between model outputs, which translates to small variability among BIOME4 simulations driven by the climate data (Figure 3.9). CCSM4 provided the coolest climate, which led to the largest simulation of shrub tundras. CCSM4 also produced more cushion forb, lichen, and moss tundra as well as graminoid tundra.

MPI-ESM and MRI-CGCM3 produced large amounts of shrub type tundras, with MRI-CGCM3 producing the most graminoid tundra of all pre-industrial simulations. The warmest simulations were provided by GISS-E2-R and MIROC-ESM, which produced the largest evergreen taiga and deciduous taiga distributions, as well as introduced warmer biomes to the region.

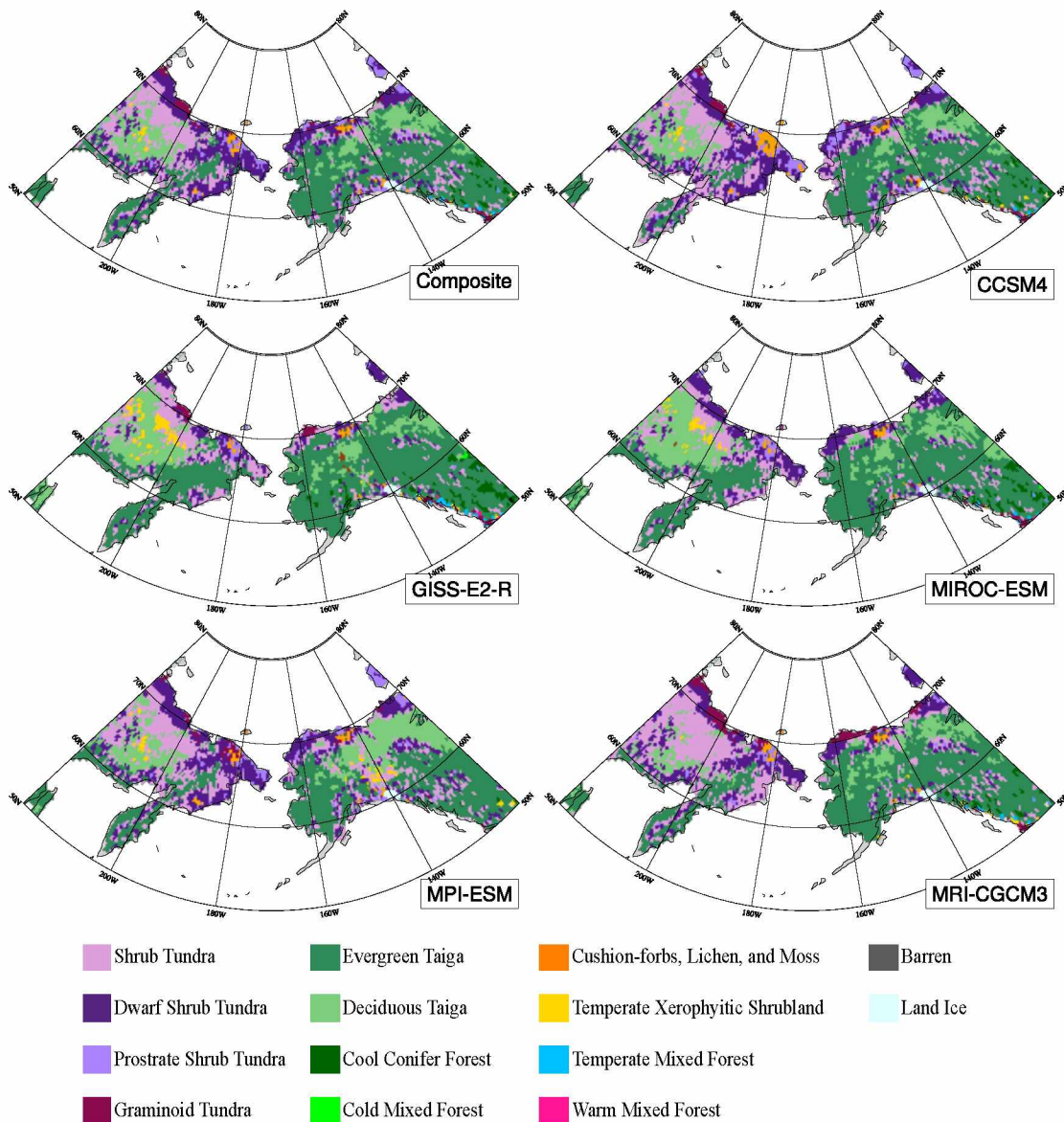


Figure 3.9 Comparison of BIOME4 pre-industrial simulations. The first map shows a summary of all five simulations. At least three models out of five were required for a composite map to produce the same biome at a grid cell with color. Black cells indicate that no single biome was simulated by at least three models.

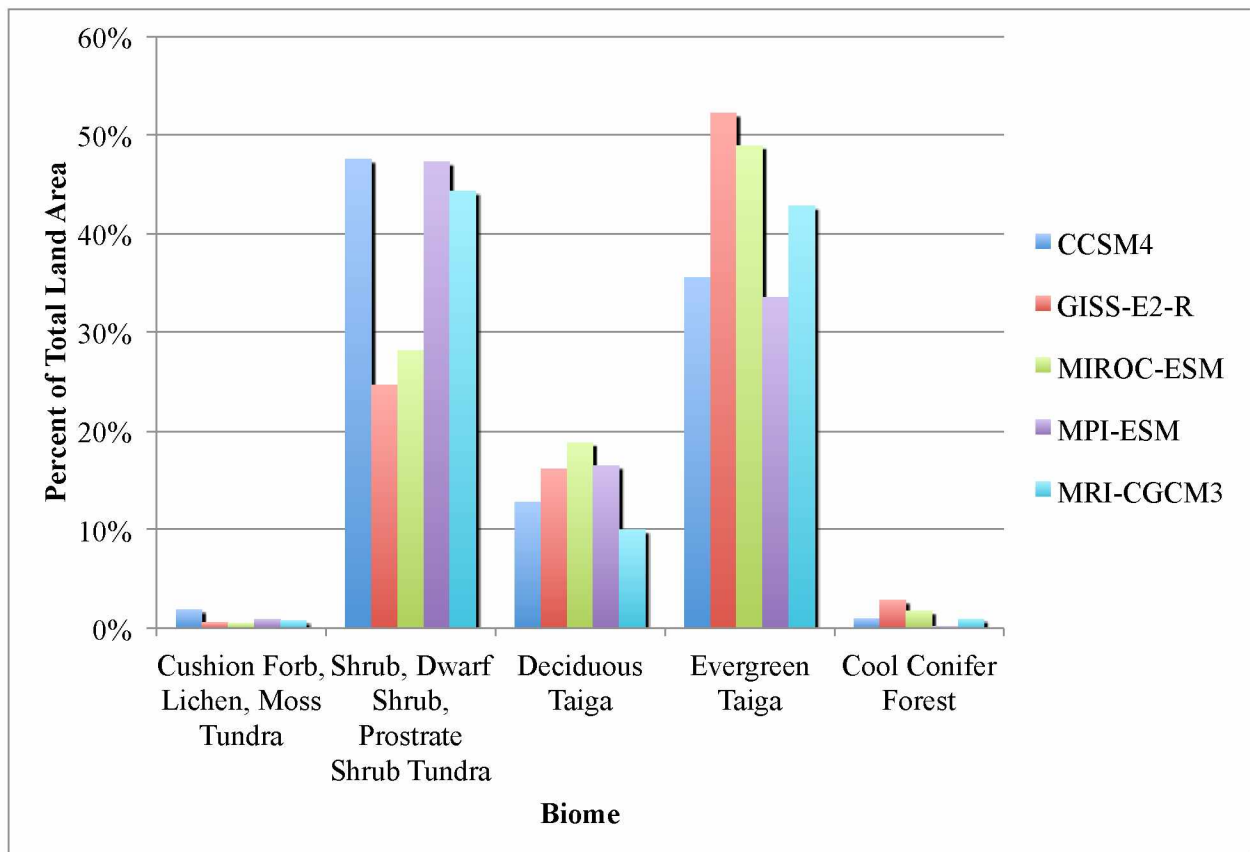


Figure 3.10 Percent of land area coverage of simulated biomes for the pre-industrial simulations.

Figure 3.10 shows the simulated biome percent of land area for each CMIP5/PMIP3 GCM. Shrub tundras and evergreen taiga dominate pre-industrial simulations. This is similar to the modern reconstruction that is also dominated by shrub tundras and evergreen taiga (Figure 3.5). Three models (CCSM4, MPI-ESM, MRI-CGCM3) simulate more shrub tundras than evergreen taiga compared to the modern reconstruction. This can be attributed to the cooler than modern climates produced by these three models. Three models produce more deciduous taiga than the modern reconstruction: GISS-E2-R, MIROC-ESM, and MPI-ESM. CCSM4 simulates a similar percent of deciduous taiga compared to the modern reconstructions, while MRI-CGCM3 simulates less deciduous taiga than the modern reconstruction.

3.3 Mid-Holocene Biome Simulations

Mid-Holocene GCM climate data shows more variability between models than the pre-industrial climate data (Figure 3.11). CCSM4 and MPI-ESM provided the coolest average seasonal summer temperatures, while GISS-E2-R and MIROC-ESM provided the warmest temperatures. MRI-CGCM3 summer temperatures are generally warmer than the modern climatology, with the exception of the southern half of the Russian study area. The corresponding GDD₀ index for each GCM is shown in Figure 3.12. The cooler CCSM4 and MPI-ESM have lower GDD₀ index values compared to the modern climatology, while the warmer GISS-E2-R and MIROC-ESM show warmer GDD₀ index values. GDD₀ index values for MRI-CGCM3 showcase the cooler temperatures in the western half with lower index values, and warmer temperatures in the eastern half with higher index values compared to modern GDD₀.

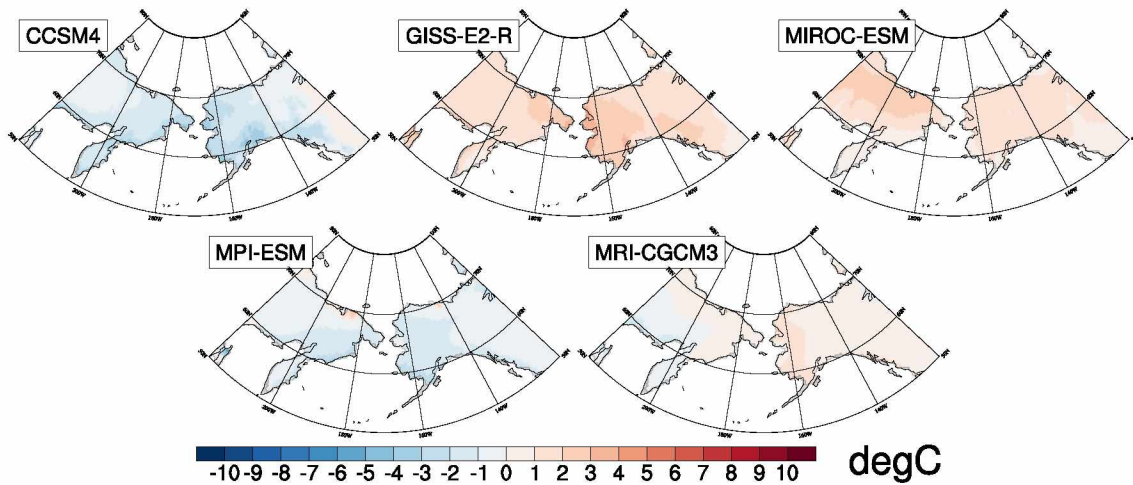


Figure 3.11 Mid-Holocene average seasonal summer (June, July, August) monthly temperature anomalies from the modern baseline climate.

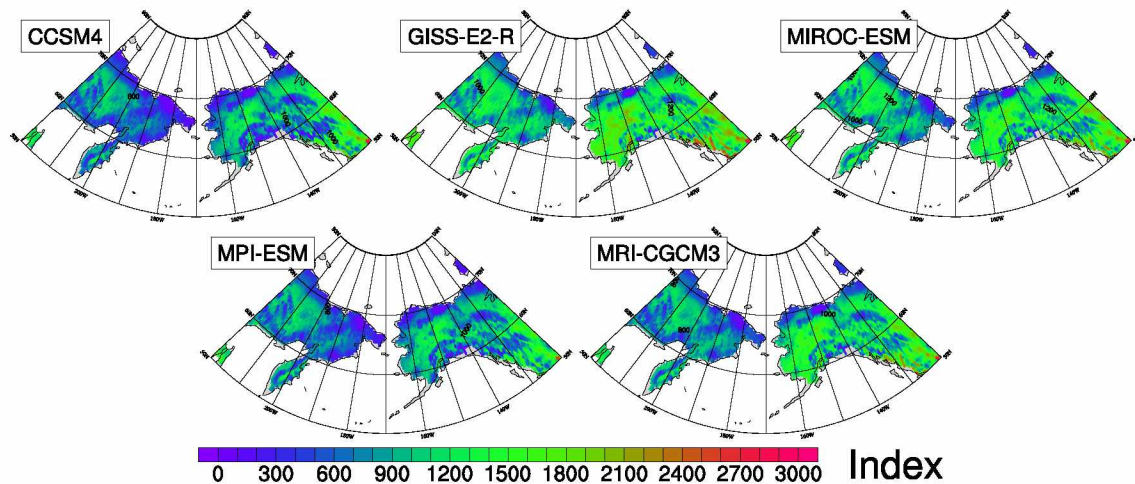


Figure 3.12 Growing degree days above 0°C for the mid-Holocene time period.

Simulated biome distributions for the mid-Holocene vary little from the modern biome reconstruction (Figure 3.13a). Nearly the entire study region is simulated to have shrub tundras or deciduous taiga or evergreen taiga, except for northern coastal areas. The composite map shows Alaska largely simulated with evergreen and deciduous taiga and is not so different from the modern reconstruction. The majority of the models put slightly more deciduous taiga in the northern portion of Alaska and western Canada. Biomes simulated in Russia are nearly identical to the modern reconstruction, with deciduous taiga placed in the interior and evergreen taiga along the southern and eastern coast. The simulated vegetation is largely shrub tundras, with very little cushion forb, lichen, and moss tundra simulated. Compared to the modern reconstruction, the mid-Holocene does not simulate any temperate xerophytic shrubland. The treeline is simulated in the same location as the modern reconstruction. While the warming of the Holocene caused the treeline to shift in some locations around the Arctic, the shift was not uniform around the pole and remained in nearly the same location in the central Beringia region (Bigelow et al., 2003; Kaufman et al., 2004). Boundaries between evergreen and deciduous taiga, and boundaries between tundra and taiga are simulated at nearly the exact same locations for both the modern reconstruction and mid-Holocene simulation.

The 6ka pollen has fewer sample locations than the 0ka map (Figure 3.13b); however, the general distribution of biomes is discernible. Interior Alaska pollen is dominated by evergreen taiga and displays the mid-Holocene treeline, with the northern and western regions displaying

shrub tundra. This contrasts with the mid-Holocene simulations where BIOME4 simulates evergreen taiga across a large portion of western Alaska and north of the Brooks Range. Pollen samples in Russia show deciduous taiga in the interior in contrast to the simulation, and pollen of shrub tundras across the eastern half. Some graminoid tundra pollen was found in the northern reaches of the study region and one sample was found in the Aleutian Islands.

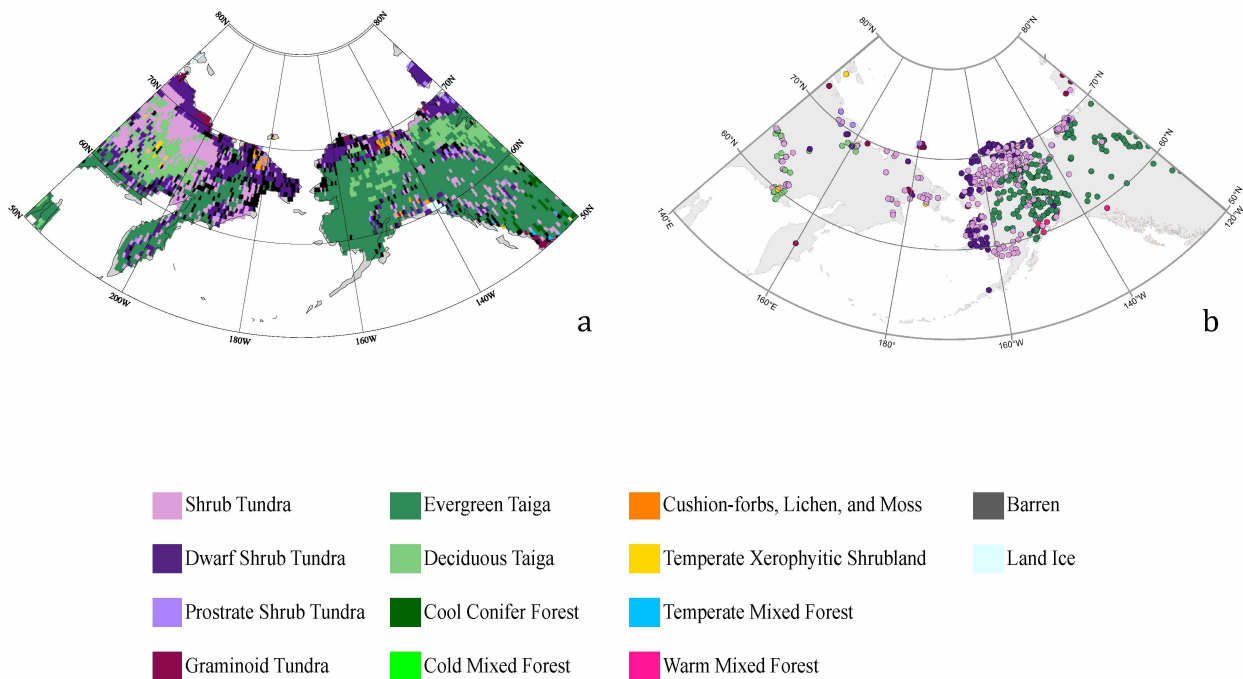


Figure 3.13 a.) Mid-Holocene summarized biome distribution map for all five CMIP5/PMIP3 GCMs; b.) pollen sample map for 6ka. At least three models out of five were required for a composite map to produce the same biome at a grid cell with color. Black cells indicate that no single biome was simulated by at least three models.

The individual mid-Holocene biome simulations are generally in good agreement, with few blacked out cells (Figure 3.14). The average seasonal summer temperature differences (Figure 3.12) can be seen in the individual simulations. CCSM4 simulated the coolest climate with the coolest biome distribution consisting of largely shrub tundra types, while GISS-E2-R which has the warmest climate, simulated the warmest biome distribution consisting of plenty of evergreen taiga and deciduous taiga. Of the five climate data sets, CCSM4, MPI-ESM, and MRI-

CGCM3 all simulated more shrub tundras especially in Russia. CCSM4 simulated the least amount of taiga across the study region; however, all simulations have similar treeline placements.

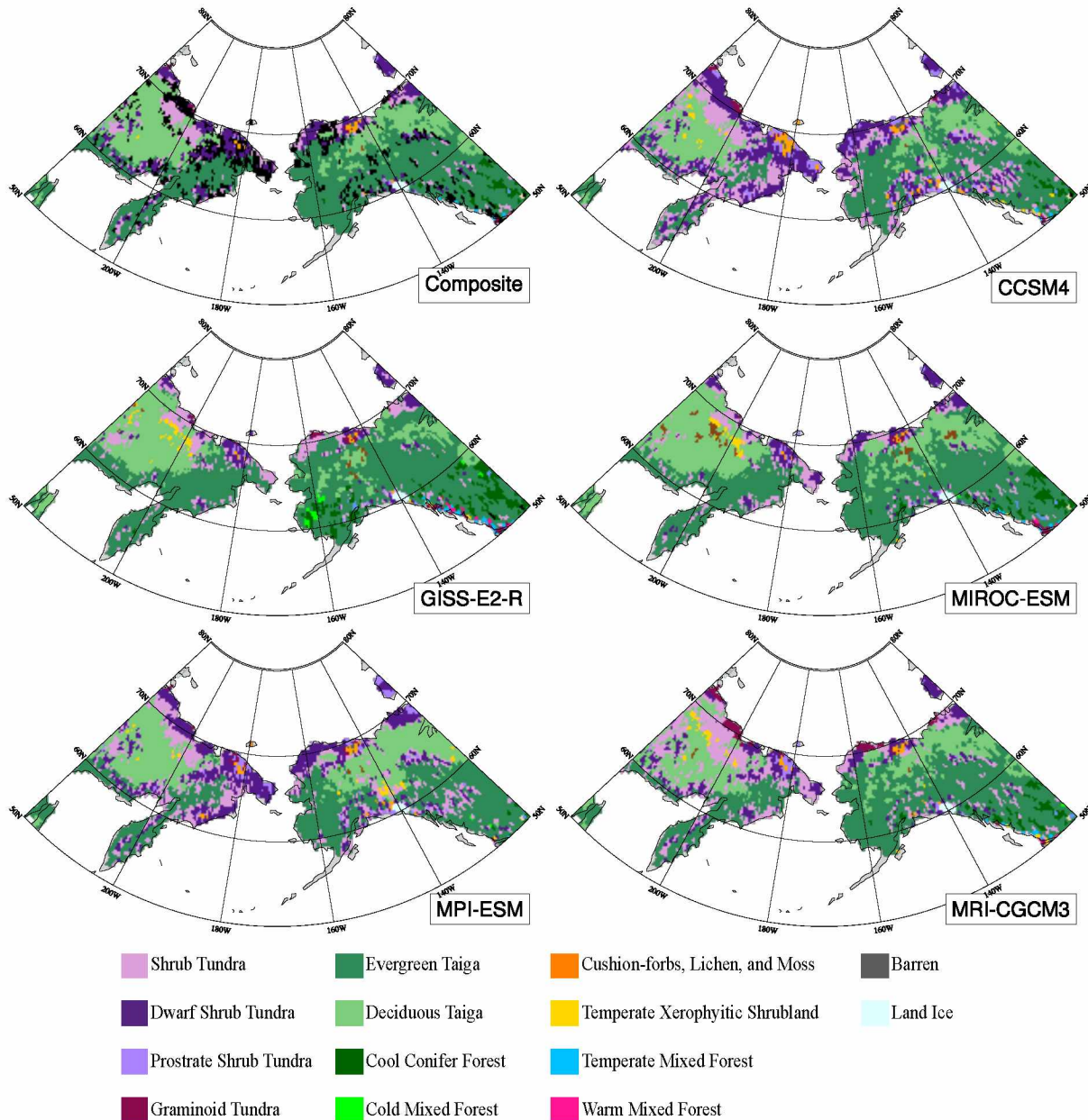


Figure 3.14 Comparison of BIOME4 mid-Holocene simulations. The first map shows a summary of all five simulations. At least three models out of five were required for a composite map to produce the same biome at a grid cell with color. Black cells indicate that no single biome was simulated by at least three models.

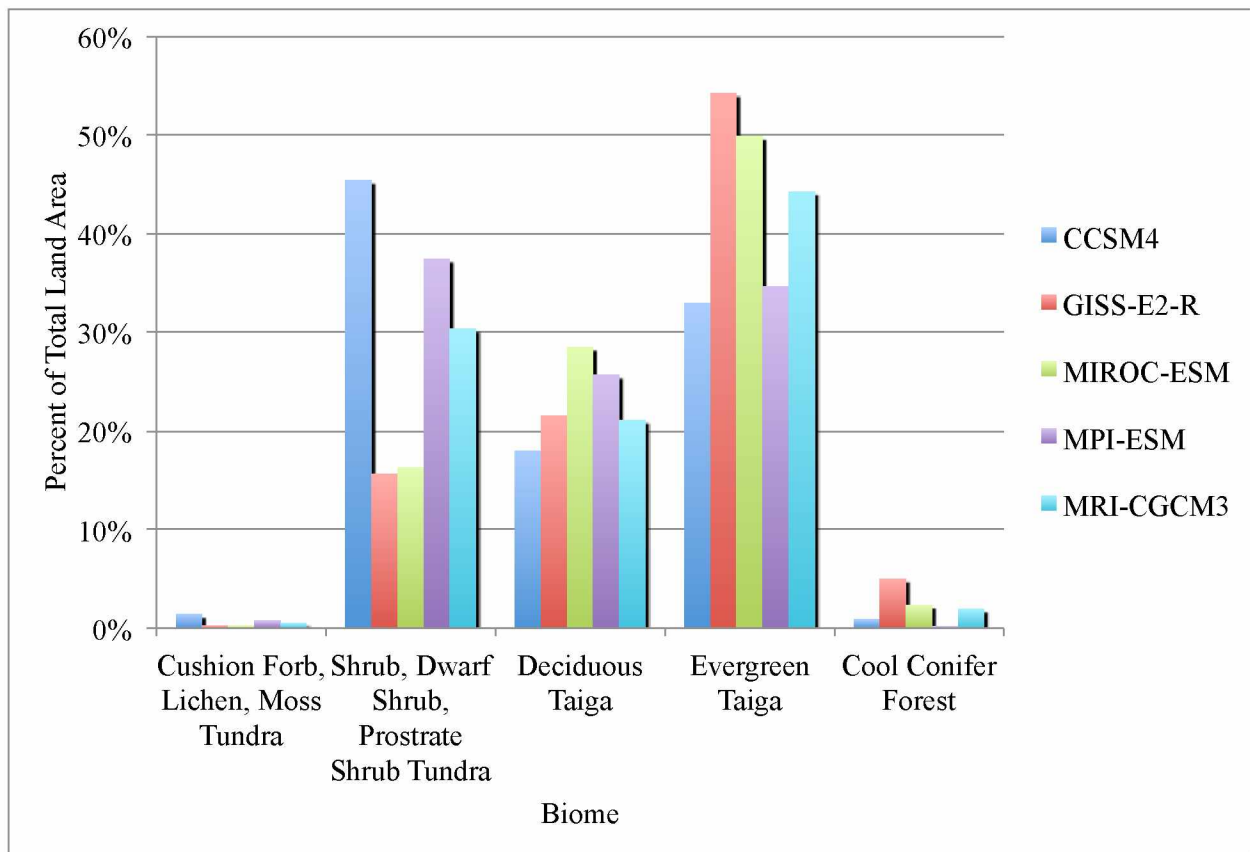


Figure 3.15 Percent of land area coverage of simulated biomes for the mid-Holocene.

Figure 3.15 shows the simulated biome percent of land area for each GCM. The mid-Holocene has slightly more variability in simulated biomes between models compared to the pre-industrial simulations (Figure 3.10). Deciduous taiga was simulated for approximately the same area percent between models within ~10%, while there is a large range between the coverage of shrub tundras (~30%) and evergreen taiga (~20%). The cooler CCSM4 produces a high percentage of shrub tundras, while the warmer GISS-E2-R produces the most evergreen taiga in the study region. More cool conifer forest was simulated for the mid-Holocene than the pre-industrial simulation and modern reconstruction.

3.4 Last Glacial Maximum Biome Simulations

Climate data for the LGM show a varying degree of cooler seasonal summer temperatures across the study region compared to the modern climatology (Figure 3.16). CCSM4, GISS-E2-R, and MIROC-ESM display cooler temperatures over non-glaciated regions compared to MPI-ESM and MRI-CGCM3. The latter two models show warmer than modern temperatures in the central and northern areas of the study region. This may be due to the interpolation of the modern climatology as station data was not available over the now-flooded ocean regions; however, research has shown that because land was exposed in central Beringia, perhaps the land bridge was warmer than present due to differences in heat capacity between land and water (Bartlein et al., 2015). Bartlein et al. (2015) found, for the early Holocene prior to the flooding of the land bridge, that eastern Beringia was cooler than Siberia due to proximity to the Laurentide ice sheet, and the land bridge provided warming during the summer. Cooler seasonal summer temperatures correspond to lower GDD_0 index values for all GCMs compared to the modern GDD_0 index values (Figure 3.17). CCSM4 and MIROC-ESM show highest index values for the LGM that are not higher than the lower values seen in the modern GDD_0 plot. GISS-E2-R, MPI-ESM, and MRI-CGCM3 all show a similar pattern of higher GDD_0 index values in the south-central region of the Bering Land Bridge. This leads to an interesting taiga biome simulation for the LGM.

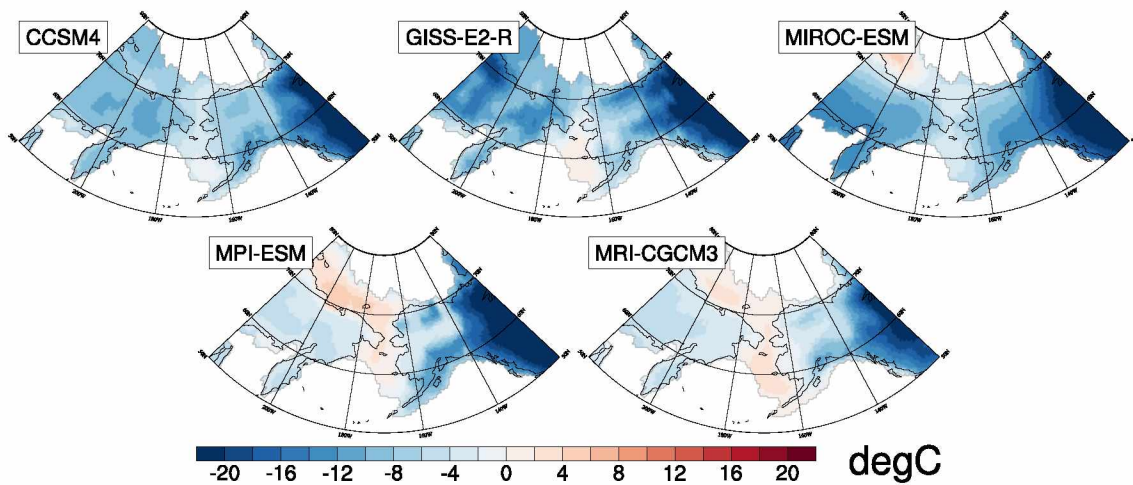


Figure 3.17 Last Glacial Maximum average seasonal summer (June, July, August) monthly temperature anomalies from modern baseline climate.

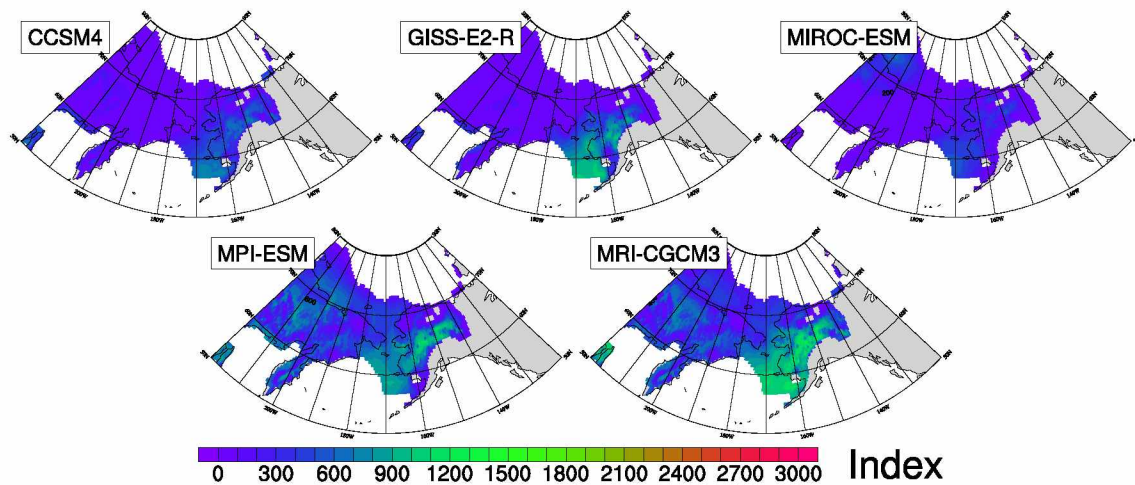


Figure 3.18 Growing degree days above 0°C for the Last Glacial Maximum. The gray areas are glaciated and were masked for these plots.

The biome distribution for the LGM is markedly different and more variable across the models compared to the other four time periods but can be matched with pollen data for 21ka (Figure 3.19). Major agreements between the models include graminoid tundra simulated along the northern shelf region, cushion forb, lichen, and moss tundra simulated across central-interior Beringia, shrub, dwarf shrub, and prostrate shrub across eastern-interior Beringia, and a small region of evergreen taiga in the south-central region of the land bridge. Ice sheets act as a barrier in the eastern portion of the study region.

The pollen map shows the study region consisted of mostly graminoid and shrub tundras. It has been noted that the possible reason for cushion forb, lichen, and moss tundra to be absent from the pollen data is “probably because the extreme conditions which favor this biome are often unfavorable for sedimentation and pollen preservation” (Kaplan et al., 2003). One interesting result is the small area of evergreen taiga simulated in the south-central Beringia region. There is no pollen data to suggest evergreen taiga existed here; however, previous simulations from BIOME4 have produced taiga in the same south-central region (Kaplan et al., 2003). Pollen based biomes are percent driven, which means if taiga existed here, there was not

enough spruce pollen in the sample to be classified as taiga. This was the same region that three of the five models showed relatively higher GDD₀ index values for the LGM.

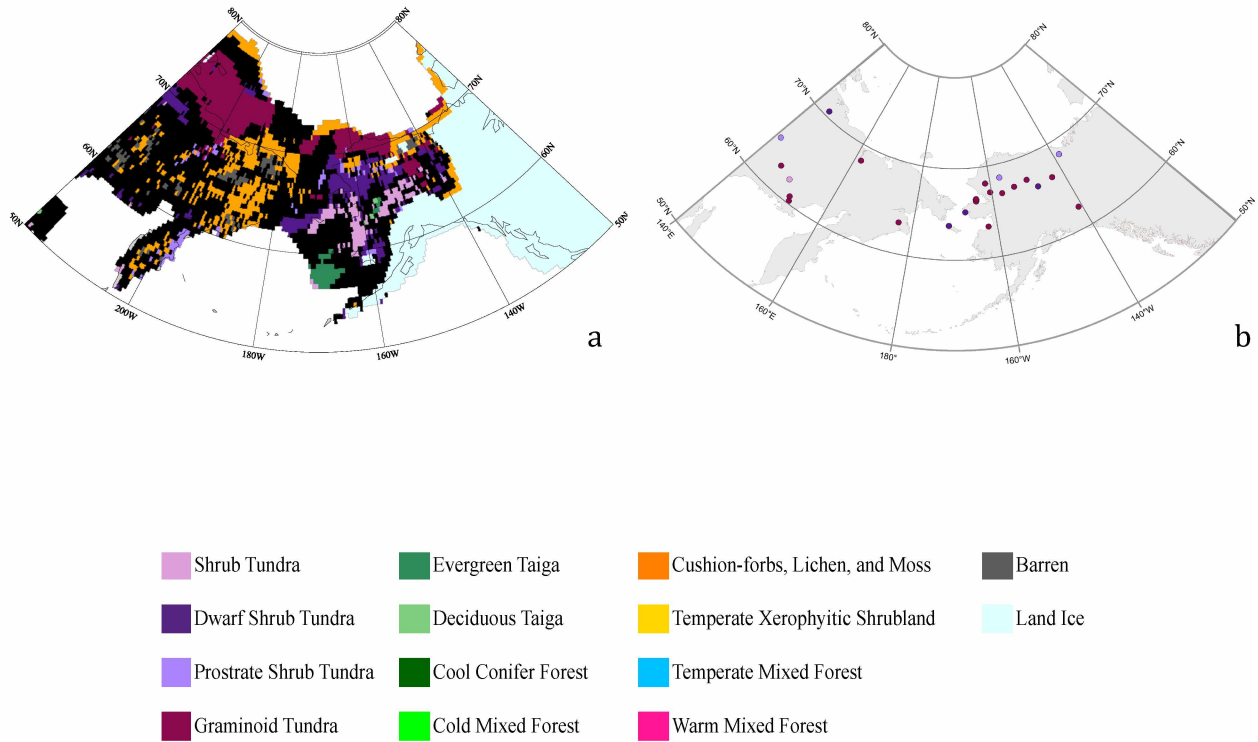


Figure 3.19 a.) Last Glacial Maximum summarized biome distribution map for all five CMIP5/PMIP3 GCMs; b.) pollen sample map for 21ka. At least three models out of five were required for a composite map to produce the same biome at a grid cell with color. Black cells indicate that no single biome was simulated by at least three models.

The LGM showed the least amount of agreement between CMIP5/PMIP3 simulations. CCSM4, GISS-E2-R, and MIROC-ESM all simulate large areas of cushion forb, lichen, and moss tundra covering the western half of Beringia, and shrub, dwarf shrub, and prostrate shrub tundra covering the eastern portion. These three models provided the coolest temperatures over non-glaciated land area (Figure 3.20). MIROC-ESM, MPI-ESM, and MRI-CGCM3 simulate large areas of graminoid tundra along the northern regions, while MIROC-ESM simulates cushion forb, lichen, and moss tundra to the west. MPI-ESM and MRI-CGCM3 simulate shrub and dwarf shrub tundra in the southern half of the study region. MPI-ESM, MRI-CGCM3, and

GISS-E2-R simulate a region of evergreen and deciduous taiga in the south-central region. MPI-ESM and MRI-CGCM3 had the warmest temperatures over non-glaciated areas, while GISS-E2-R had cooler temperatures except for the middle region where taiga was simulated.

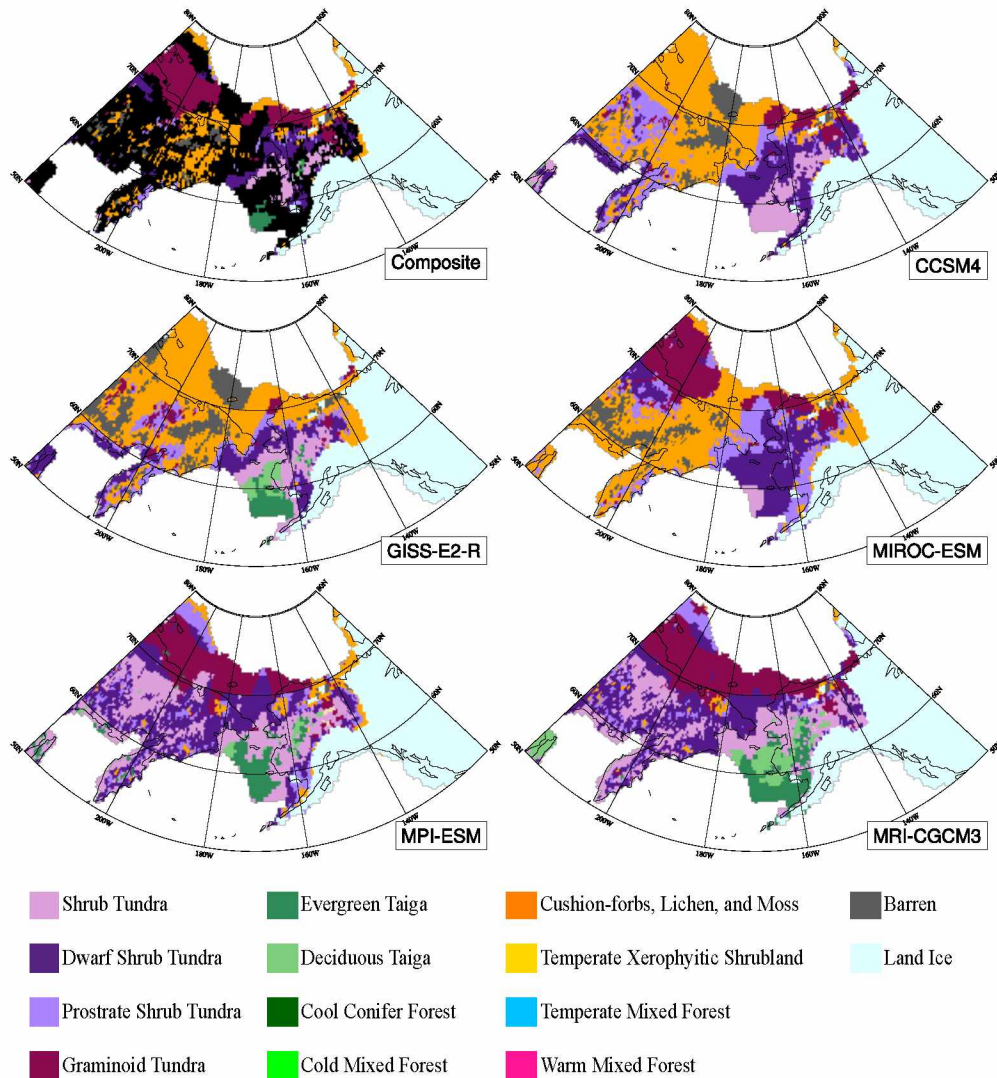


Figure 3.20 Comparison of BIOME4 Last Glacial Maximum simulations. The first map shows a summary of all five simulations. At least three models out of five were required for a composite map to produce the same biome at a grid cell with color. Black cells indicate that no single biome was simulated by at least three models.

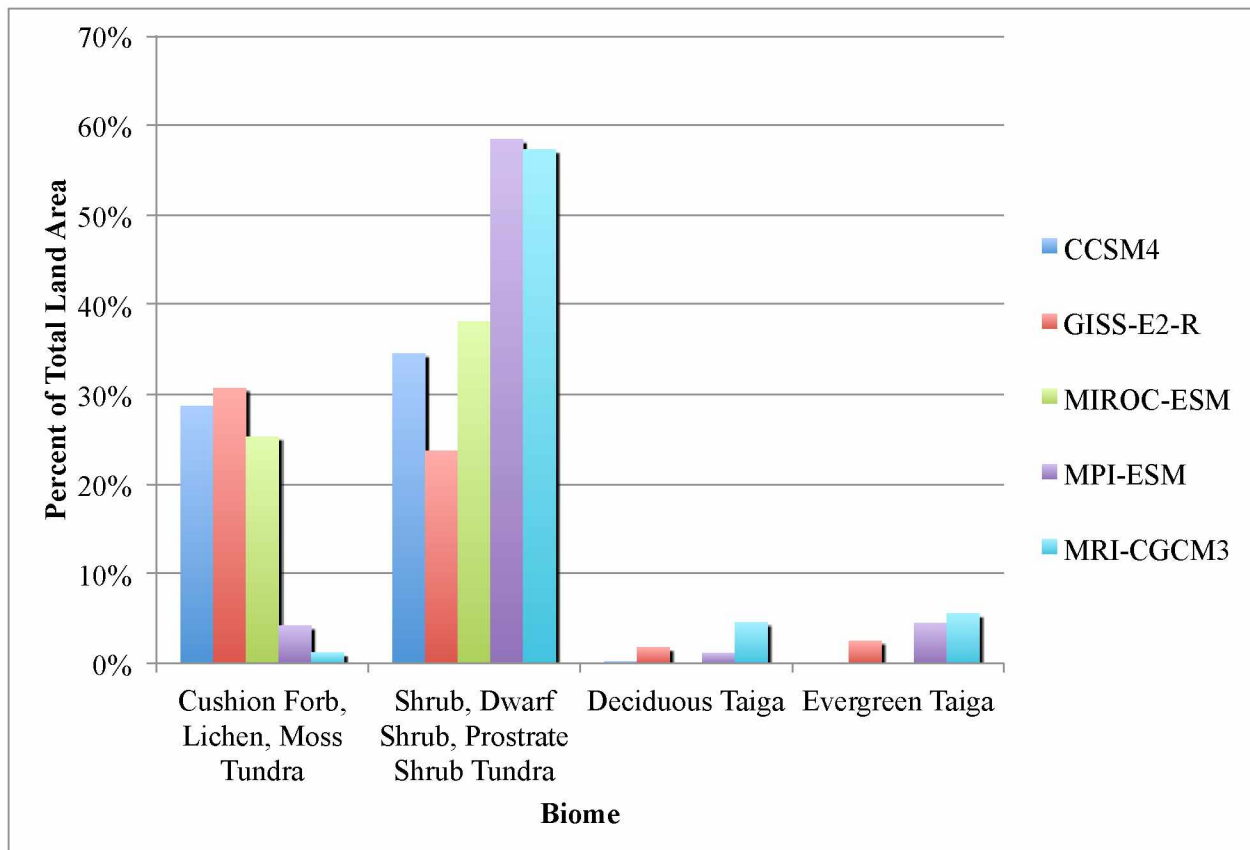


Figure 3.21 Percent of land area coverage of simulated biomes for the Last Glacial Maximum.

Figure 3.21 displays the percent of land area coverage for the LGM. CCSM4, GISS-E2-R, and MIROC-ESM all simulated relatively similar coverage of cushion forb, lichen, and moss tundra and shrub tundras. MPI-ESM and MRI-CGCM3 simulated the least amount of cushion forb, lichen, and moss tundra, and high coverage of shrub tundras. MPI-ESM and MRI-CGCM3 also simulated the most taiga, with GISS-E2-R also simulating taiga.

3.5 Future Biome Simulations

Future climate data based on the IPCC RCP 8.5 scenario show warmer temperatures over the 21st century for all five GCMs (Figure 3.22). CCSM4 and MIROC-ESM show the warmest average seasonal summer temperatures. MPI-ESM and MRI-CGCM3 show the least warming in the future, with MPI-ESM showing very weak warming across Alaska, and MRI-CGCM3

showing the same in the eastern Russian section of the study region. The warmer summer temperatures from all GCMs correspond to increased GDD_0 index values for all GCMs compared to modern GDD_0 values (Figure 3.23). The warmest CCSM4 and MIROC-ESM show high index values in Interior Alaska and Canada. GISS-E2-R, MPI-ESM, and MRI-CGCM3 show similar GDD_0 index values, with increased areas of the larger index values across the study region.

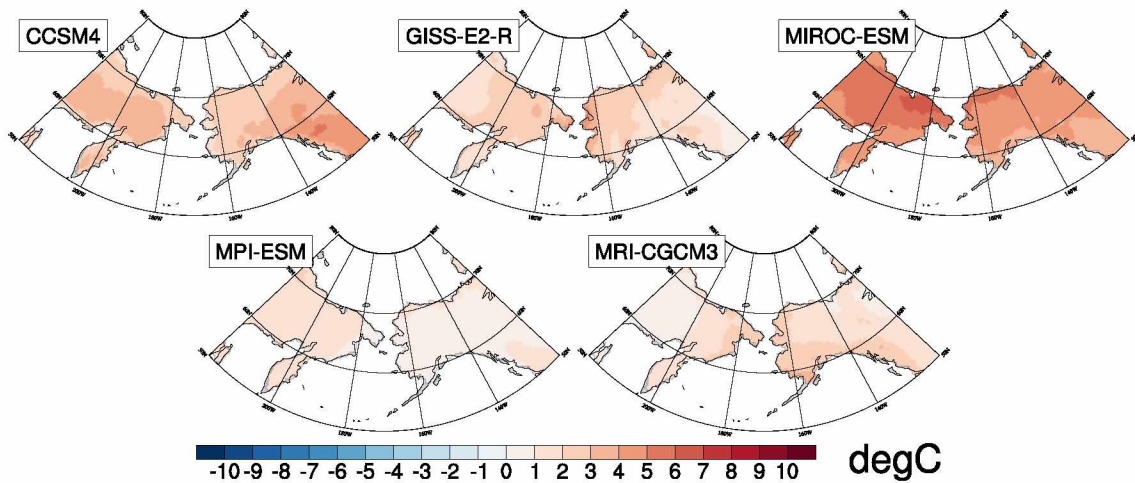


Figure 3.22 RCP 8.5 average seasonal summer (June, July, August) temperature anomalies from modern baseline climate.

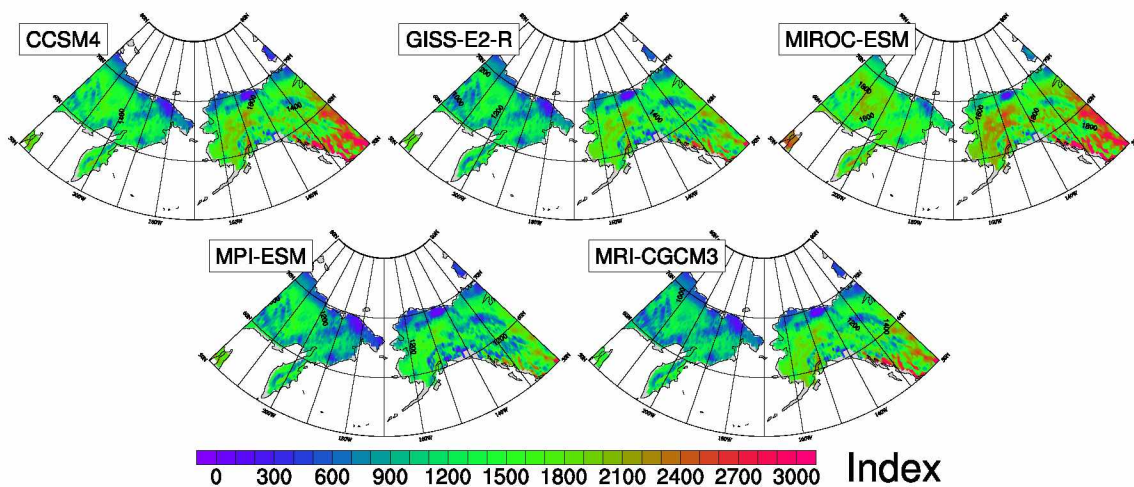


Figure 3.23 Growing degree days above 0°C for the IPCC RCP 8.5 climate projections.

Warmer summer temperatures translate to BIOME4 simulated reductions in tundra area, increases in evergreen and deciduous taiga area, as well as a northward expansion of warmer biome types from the south (Figure 3.24) compared to the modern biome reconstruction (Figure 3.1). Most of the study region is simulated to have evergreen or deciduous taiga under future climate conditions. It's important to remember that BIOME4 is an equilibrium vegetation model, whereas projected future climate scenarios are transient. Vegetation does not react to climate change as quickly as climate change occurs. Like the modern day reconstruction, and pre-industrial, and mid-Holocene simulations, deciduous taiga is produced in interior Russia with evergreen taiga along the edges. The simulations in Alaska and Canada largely have evergreen taiga across the region. Warmer biome types, such as cool conifer forest, and warm and cool mixed forests are simulated in the Interior and southwest Alaska regions, as well as southern Yukon Territory and British Columbia. Tundra type biomes are almost absent in the future simulation but still maintain land coverage in the northern boundaries of the study region. One thing to note is the treeline reaching the Arctic coast in the future simulations. This agrees with previous simulations done at an increase of 2°C in the Arctic (Kaplan and New, 2006). A few small areas along the coast continue to simulate shrub tundras.

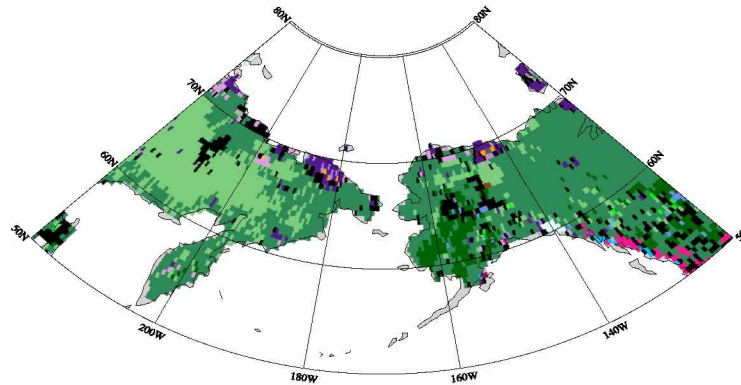


Figure 3.24 RCP 8.5 summarized biome distribution map. At least three models out of five were required for a composite map to produce the same biome at a grid cell with color. Black cells indicate that no single biome was simulated by at least three models.

Future biome projections display less variability than pre-industrial, mid-Holocene, and especially LGM simulations, showing cohesion among the selected CMIP5 models for future climate projections (Figure 3.25). CCSM4 and MIROC-ESM produced the warmest summer climate (Figure 3.22), bringing with it warmer biomes including temperate mixed forest and warmed mixed forest. Cool conifer forest is projected in southwest Alaska; however, the accuracy of this placement could be in question considering the disparity in this area for all time periods. Only MPI-ESM did not produce significant cool conifer forest coverage with its coolest summer temperatures. MPI-ESM and MRI-CGCM3 retained the largest percent area of shrub tundras, while MIROC-ESM projected virtually no shrub tundras. The differences in timing of the GCM simulations from GISS-E2-R and MPI-ESM (the former for the early part of the

century and the latter for the end of the century) did not produce major differences in biome simulations. GISS-E2-R climate data simulated more conifer forest in the western part of Alaska but is consistent with simulations from CCSM4 and MRI-CGCM3. MPI-ESM climate data simulated a biome distribution that is very similar to the modern biome reconstruction and not the warmer biome distribution I expected with climate data from the latter part of the 21st century.

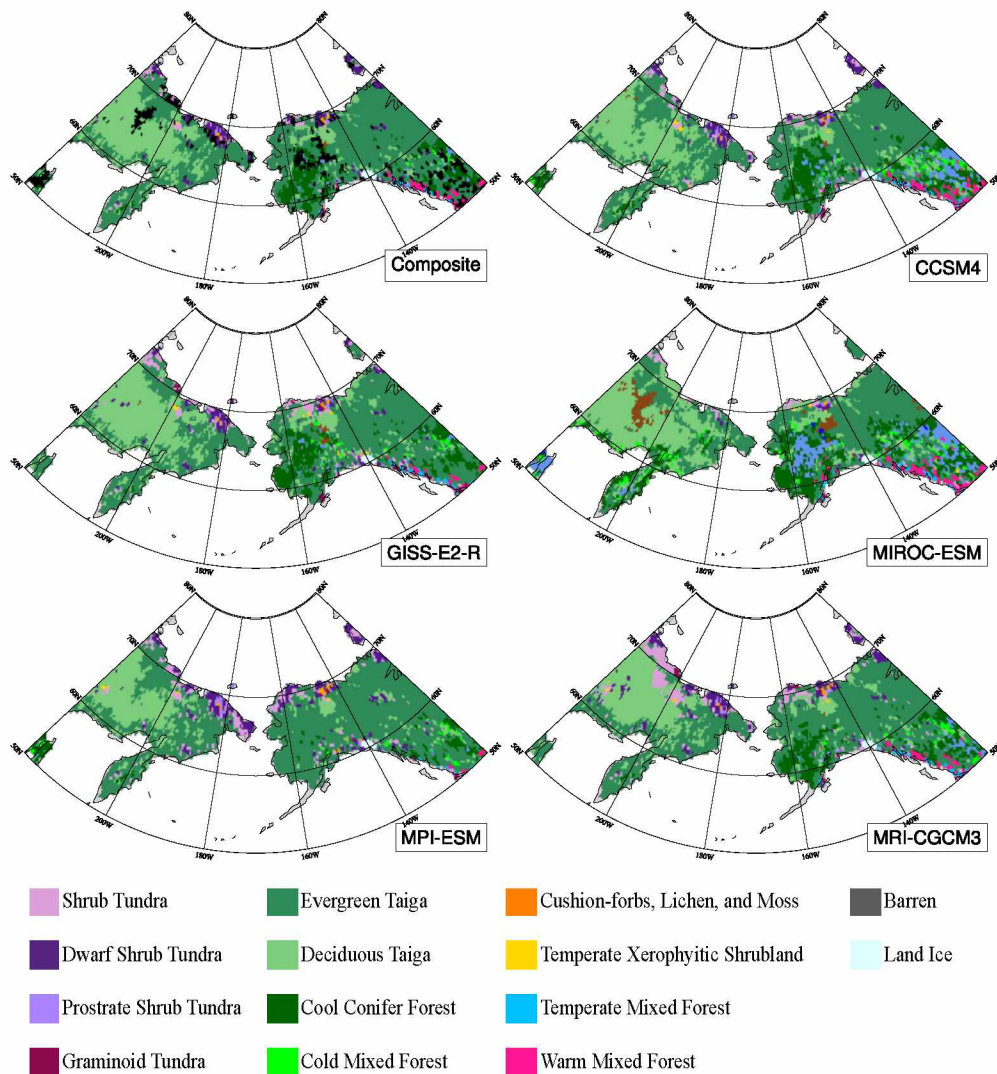


Figure 3.25 Comparison of BIOME4 RCP 8.5 projections. The first map shows a summary of all five simulations. At least three models out of five were required for a composite map to produce the same biome at a grid cell with color. Black cells indicate that no single biome was simulated by at least three models.

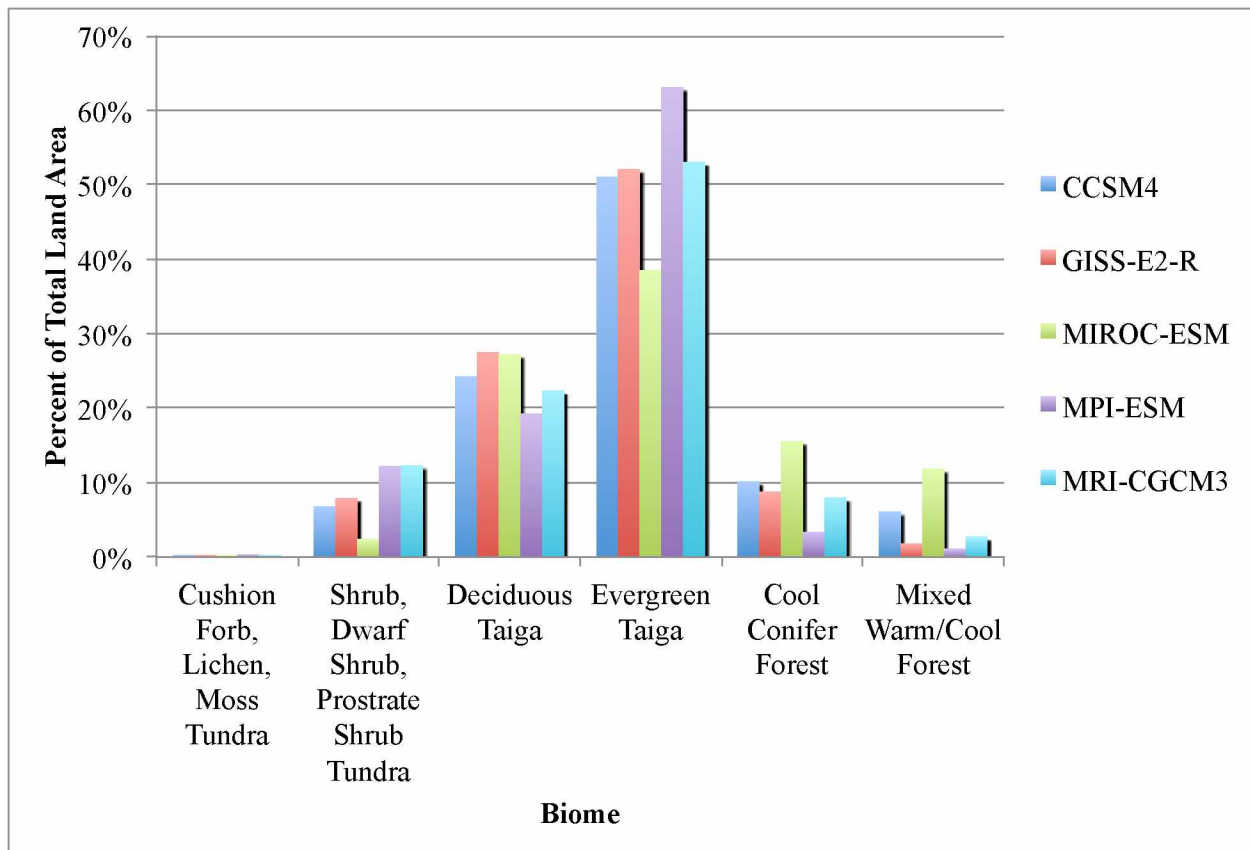


Figure 3.26 Percent of land area coverage for RCP 8.5 climate projections.

Figure 3.26 displays the percent of land area coverage for the RCP 8.5 climate. Individual simulations were in generally good agreement so the percent distributions are equally in good agreement. One major difference is the results from MIROC-ESM. This model provided the warmest temperatures for RCP 8.5 climate, so simulated the least shrub tundras, and the highest coverage of warmer biomes, cool conifer forest and mixed warm and mixed cool forests.

3.6 Sensitivity Analysis

Each biome appears to have an optimal range of temperature for simulation (Figure 3.27). In the temperature sensitivity experiment, precipitation was unchanged from the present day values. The modern baseline climate monthly temperatures were changed in 2°C increments to investigate the sensitivity of biomes simulated by BIOME4 in response to the temperature variations. Cushion forb, lichen, and moss tundra is the most cold tolerant plant type, followed

by shrub tundras, evergreen taiga, deciduous taiga, and cool conifer forest. Warm biome types appear in the region with just 2°C warming from the modern climatology. Since the Arctic can be quite dry, it makes sense that as temperatures warm and precipitation is held constant, a desert biome appears in the study region. The modern biome distribution does not fit with the temperature regime trend, showing a disproportionately high percent of evergreen taiga though the adjacent ($\pm 2^\circ\text{C}$) regime, which would indicate more deciduous taiga should exist. The schematic shown in Figure 2.5 shows the bioclimatic limits of biomes used BIOME4. It is interesting to note the increase in deciduous taiga with warming in the sensitivity experiment though the limits are on the temperature of the coldest month, where deciduous taiga is limited to areas with colder winters than even evergreen taiga. However, the mid-Holocene simulations, which are characterized by warmer summer temperatures than present day, also show an expanded deciduous taiga. BIOME4 was optimized for the current Arctic climate and this could explain why incremental changes in temperature produce decidedly different biome distributions than the modern reconstruction. This raises the question of how well can BIOME4 accurately simulate other time periods if it was optimized for the current climate; however, the simulations for the pre-industrial, mid-Holocene, and LGM biome distributions show relatively good agreement with pollen data.

Arctic biomes as simulated by BIOME4 are not as sensitive to precipitation changes (Figure 3.28). In the precipitation sensitivity experiment, temperature was unchanged from the present day values. Deciduous taiga appears the most sensitive to precipitation changes. However, for a 60% range in precipitation changes, deciduous taiga coverage changes ~5%. All other biomes present in the simulations show very little if any sensitivity to increases or decreases in precipitation. These relationships between the sensitivity of biomes in BIOME4 to temperature and precipitation changes agree with what is known about the relationship between climate and Arctic vegetation: that Arctic vegetation is driven more strongly by temperature than by any other climate variable (CAVM, 2003).

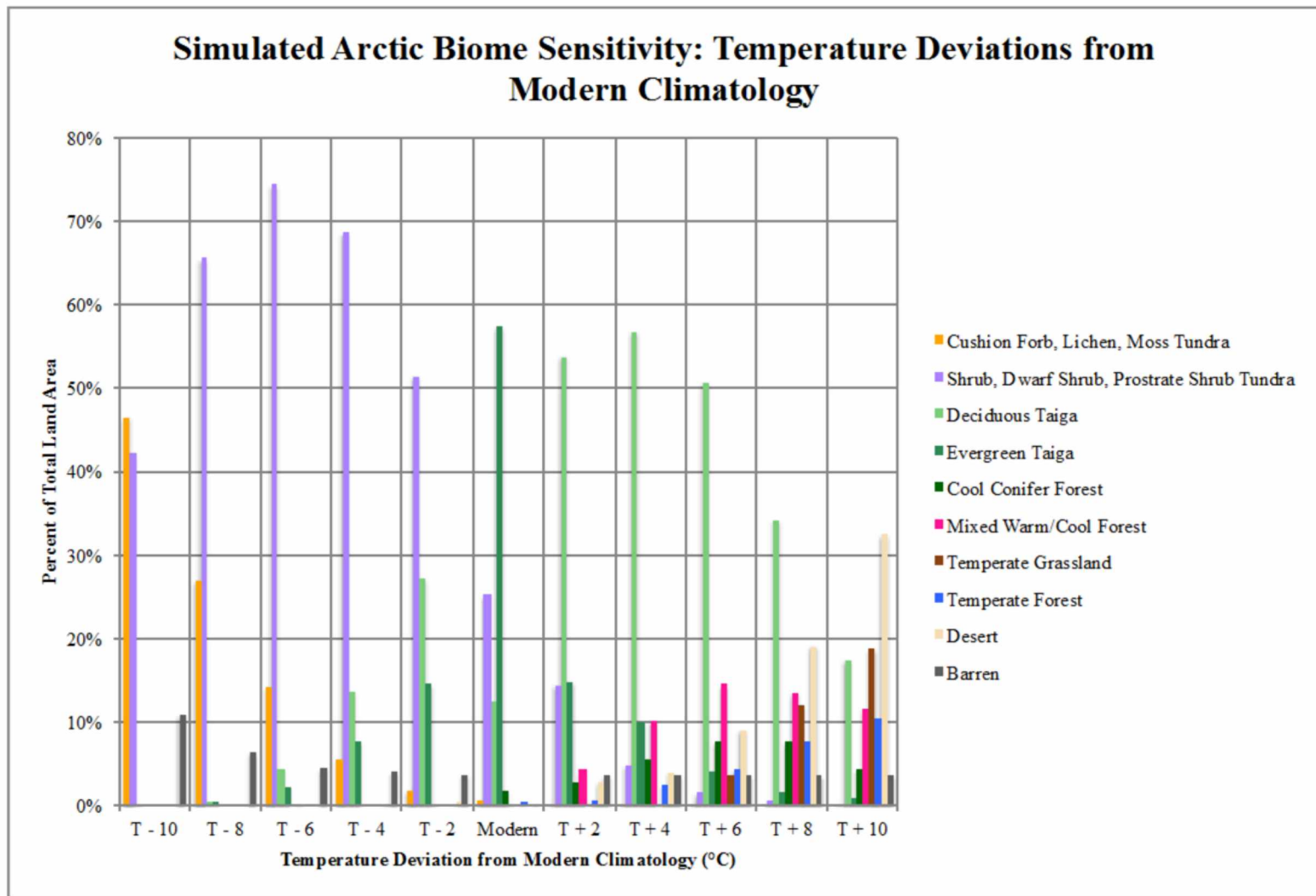


Figure 3.27 Simulated Arctic biome sensitivity to temperature changes. The horizontal axis shows the incremental temperature changes in the modern climatology, and the vertical axis shows the percent of land area occupied by biomes.

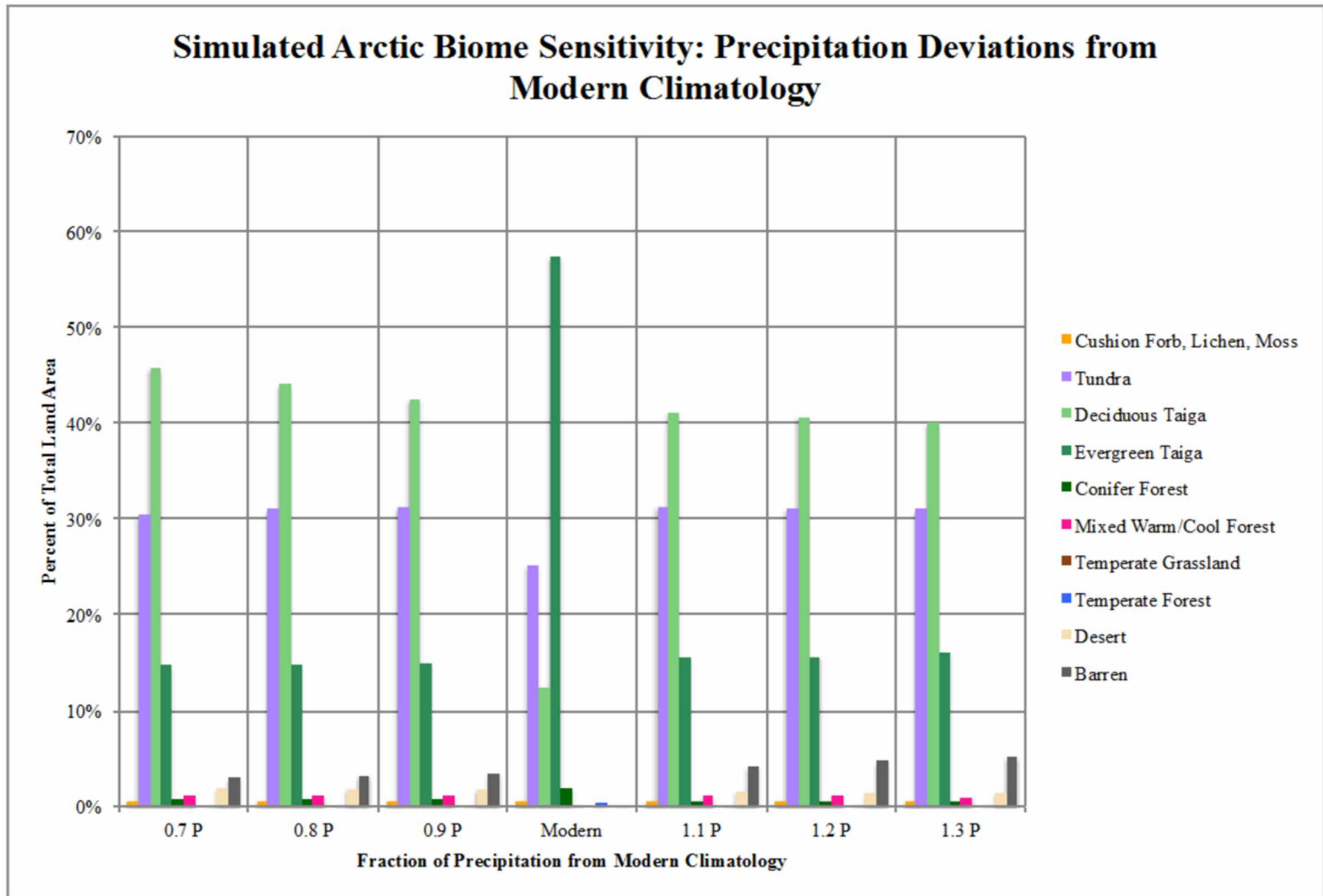


Figure 3.28 Simulated Arctic biome sensitivity to precipitation changes. The horizontal axis shows the incremental temperature changes in the modern climatology, and the vertical axis shows the percent of land area occupied by biomes.

4. Summary and Conclusions

To summarize we return to the questions prompted at the beginning of this thesis.

1. How well is Arctic vegetation simulated during the Late Quaternary period under different climate conditions?

Arctic biome distributions simulated by BIOME4 for the modern, pre-industrial, mid-Holocene, Last Glacial Maximum climates were found to be in agreement with observations, dated paleo-pollen samples, and previous research. The relationship that growing season temperature drives Arctic vegetation can be seen in the biome simulations. The modern climatology simulation captures the modern day vegetation distribution at the large scale. However, through reconstructing the modern biome distribution, I noticed a few regions where BIOME4 does not simulate the proper biome. These regions are north of the Brooks Range and western and southwestern Alaska. BIOME4 simulates taiga where shrub type tundra physically exists.

2. How sensitive are simulated biomes to changes in climate?

Arctic biomes are more sensitive to temperature changes than to other single climate variables such as precipitation. Biomes occupy a range of temperatures but all have an optimal temperature for simulation. Large changes in precipitation were not found to alter the biome distributions. Simulations for the pre-industrial time period were in general agreement with the treeline simulated slightly south of its modern day position as well as a larger expanse of shrub type tundras. Southwest Alaska is again simulated as evergreen taiga but the pollen data does not support the simulation. Pollen data for the pre-industrial time period shows much more shrub type tundra than is simulated by BIOME4. The mid-Holocene simulations were also in good agreement between GCMs. The treeline is in a similar location to modern day, and the entire region is largely taiga. Shrub type tundra is greatly reduced and there is very little cushion forb, lichen, and moss tundra. The LGM biome simulations displayed the least amount of agreement between CMIP5/PMIP3

GCMs. Much of the area is simulated to have cushion forb, lichen, and moss tundra, graminoid tundra, or shrub type tundra. A small area in south-central Beringia is simulated to have taiga but the pollen data does not support this.

3. What are the future projections of Arctic vegetation under the IPCC RCP 8.5 climate scenario and consequent impacts?

A steady-state biome distribution corresponding to future warming climate projections show the Arctic becoming greener with increases in evergreen taiga and deciduous taiga, both of which are simulated to exist at the Arctic coast. All tundra type biomes are greatly reduced in the future, with only a few small areas projected to still have tundra. Warmer biomes begin to migrate much farther than previous climates have allowed. Future biome projections show very good agreement between CMIP5 models indicating high confidence in the climate projections for the 21st century under IPCC's RCP 8.5 scenario. The projections agree with previous simulations conducted for another warmer climate scenario (Kaplan and New, 2006).

The results presented in this thesis have potential to be used in future research projects looking at climate-vegetation-permafrost dynamics. Future work could include translating simulated biome distributions to soil organic layer depth for the use in subsurface models that simulate changes in permafrost and hydrology. The biome distributions could also be used to explore changes in land-surface dynamics such as evapotranspiration, albedo, and carbon exchanges.

5. References

- ACIA, 2005: Impacts of a Warming Arctic: Arctic Climate Impact Assessment. Cambridge University Press, 139 pp.
- Bartlein, P. J., M.E. Edwards, S.W. Hostetler, S.L. Shafer, P.M. Anderson, L.B. Brubaker, and A.V. Lozhkin, 2015: Early-Holocene warming in Beringia and its mediation by sea-level and vegetation changes. *Clim. Past*, **11**, 873-932.
- Bieniek, P.A., U.S. Bhatt, R.L. Thoman, H. Angeloff, J. Partain, J. Papineau, F. Frisch, E. Holloway, J.E. Walsh, C. Daly, M. Shulski, G. Hufford, D.F. Hill, S. Calos, and R. Gens, 2012: Climate Divisions for Alaska Based on Objective Methods. *J. Appl. Met. and Clim.*, **51**, doi:10.1175/JAMC-D-11-0168.1.
- Bigelow, N.H., L.B. Brubaker, M.E. Edwards, S.P. Harrison, I.C. Prentice, P.M. Anderson, A.A. Andreev, P.J. Bartlein, T.R. Christensen, W. Cramer, J.O. Kaplan, A.V. Lozhkin, N.V. Matveyeva, D.F. Murray, A.D. McGuire, V.Y. Razzhivin, J.C. Ritchie, B. Smith, D.A. Walker, K. Gajewski, V. Wolf, B.H. Holmqvist, Y. Igarashi, K. Kremenetskii, A. Paus, M.F.J. Pisaric, and V.S. Volkova, 2003: Climate change and Arctic ecosystems: 1. Vegetation changes north of 55°N between the last glacial maximum, mid-Holocene, and present. *J. Geophys. Res.*, **108**, doi: 10.1029/2002D002558.
- Boggs, K., T.V. Boucher, and T. Kuo, 2014a: Vegetation Map and Classification: Southern Alaska and Aleutian Islands. Alaska Natural Heritage Program, University of Alaska Anchorage, Anchorage. <http://aknhp.uaa.alaska.edu>.
- Boggs, K., T.V. Boucher, and T. Kuo, 2014b: Vegetation Map and Classification: Northern, Western and Interior Alaska. Alaska Natural Heritage Program, University of Alaska Anchorage, Anchorage. <http://aknhp.uaa.alaska.edu>.

Braconnot, P., S.P. Harrison, M. Kageyama, P.J. Bartlein, V. Masson - Delmotte, A. Abe-Ouchi, B. Otto-Bliesner, and Y. Zhao, 2012: Evaluation of climate models using palaeoclimatic data. *Nat. Clim. Chan.* **2**, 417-424.

Brovkin, V., L. Boysen, T. Raddatz, V. Gayler, A. Loew, and M. Claussen, 2013: Evaluation of vegetation cover and landsurface albedo in MPI-ESM CMIP5 simulations. *J. Adv. Model. Earth Syst.*, **5**, 48–57, doi:10.1029/2012MS000169.

Cannonne, N, J.C. Ellis Evans, R. Strachan, and M. Guglielmin, 2006: Interactions between climate, vegetation and the active layer in soils at two Maritime Antarctic sites. *Antarc. Sci.*, **18**, 323-333. DOI 10.1017/S095410200600037X

CAVM Team, 2003. Circumpolar Arctic Vegetation Map. (1:7,500,000 scale), Conservation of Arctic Flora and Fauna (CAFF) Map No. 1. U.S. Fish and Wildlife Service.

Edwards, M. E., P. M. Anderson, L. B. Brubaker, T. A. Ager, A. A. Andreev, N. H. Bigelow, L. C. Cwynar, W. R. Eisner, S. P. Harrison, F.-S. Hu, D. Jolly, A. V. Lozhkin, G. M. MacDonald, C. J. Mock, J. C. Ritchie, A. V. Sher, R. W. Spear, J. W. Williams, and G. Yu, 2000: Pollen-Based Biomes for Beringia 18,000, 6000 and 0 ¹⁴C yr BP. *J. of Biogeo.* **27**, 521-554.

Garsia, M.G., ed, 1990: The Forests of the USSR: Map Scale 1:2500000, prepared by the department of the forest cartography of Souzgiptosleskhoza. Moscow: GUGK.

Gent, P.R., G. Danabasoglu, L.J. Donner, M.M. Holland, E.C. Hunke, S.R. Jayne, D.M. Lawrence, R.B. Neale, P.J. Rasch, M. Vertenstein, P.H. Worley, Z. Yang, and M. Zhang, 2011: The Community Climate System Model Version 4. *J. Clim.*, **24**, 4973-4991.

Haxeltine, A., and I.C. Prentice, 1996: BIOME3: An equilibrium terrestrial biosphere model based on ecophysiological constraints, resource availability, and competition among plant functional types. *Glob. Biogeochem. Cyc.*, **10**, 693-709.

Hopkins, D.M., J.V. Matthews, and C.E. Schweger (eds.), 1982: *Paleoecology of Beringia*. Academic Press, New York, NY, 504 pp.

IPA, accessed 2015: What Is Permafrost?

[<http://ipa.arcticportal.org/publications/occasional-publications/what-is-permafrost>]

IPCC, 2013: Climate Change 2013: The Physical Science Basis. Contribution of Working Group I to the Fifth Assessment Report of the Intergovernmental Panel on Climate Change. Cambridge University Press, Cambridge, United Kingdom and New York, NY, USA.

IPCC, 2007: The Physical Science Basis. Contribution of Working Group I to the Fourth Assessment Report of the Intergovernmental Panel on Climate Change. Cambridge University Press, Cambridge, United Kingdom and New York, NY, USA.

Kaplan, J.O. and M. New, 2006: Arctic climate change with a 2°C global warming: Timing, climate patterns, and vegetation change. *J. Clim. Change*, **79**, 213-241.

Kaplan, J.O., N.H. Bigelow, I.C. Prentice, S.P. Harrison, P.J. Bartlein, T.R. Christensen, W. Cramer, N.V. Matveyeva, A.D. McGuire, D.F. Murray, V.Y. Razzhivin, B. Smith, D.A. Walker, P.M. Anderson, A.A. Andreev, L.B. Brubaker, M.E. Edwards, and A.V. Lozhkin, 2003: Climate change and Arctic ecosystems: 2. Modeling, paleo-model comparisons, and future projections. *J. Geophys. Res.*, **108**, doi: 10.1029/2002D002559.

Kaufman, D.S., D.P. Schneider, N.P. McKay, C.M. Ammann, R.S. Bradley, K.R. Briffa, G.H. Miller, B.L. Otto-Bliesner, J.T. Overpeck, B.M. Vinther, and Arctic Lakes 2k

Project Members, 2009: Recent Warming Reverses Long-Term Arctic Cooling. *Science*, **325**, 1236 - 1239.

Kaufman, D.S., T.A. Ager, N.J. Anderson, P.M. Anderson, J.T. Andrews, P.J. Bartlein, L.B. Brubaker, L.L. Coats, L.C. Cwynar, M.L. Duvall, A.S. Dyke, M.E. Edwards, W.R. Eisner, K. Gajewski, A. Geirsdóttir, F.S. Hu, A.E. Jennings, M.R. Kaplan, M.W. Kerwin, A.V. Lozhkin, G.M. MacDonald, G.H. Miller, C.J. Mock, W.W. Oswald, B.L. Otto-Bliesner, D.F. Porinchu, K. Rühland, J.P. Smol, E.J. Steig, and B.B. Wolfe, 2004: Holocene thermal maximum in the western Arctic (0-180°W). *Quat. Sci. Rev.*, **23**, 529-260.

Matsuura, K. and C.J. Willmott, 2009a: Terrestrial Air Temperature: 1900-2008 Gridded Monthly Time Series (Version 2.01). Center for Climatic Research, University of Delaware.

Matsuura, K. and C.J. Willmott, 2009b: Terrestrial Precipitation: 1900-2008 Gridded Monthly Time Series (Version 2.01). Center for Climatic Research, University of Delaware.

NSIDC, 2015: All About Frozen Ground. Accessed May 2015. [Available online at <https://nsidc.org/cryosphere/frozenground/index.html>.]

Rekacewicz, P., UNEP/GRID-Arendal, 1998, cited 2015: Circumpolar Active-Layer Permafrost System (CAPS), version 1. [Available online at https://nsidc.org/sites/nsidc.org/files/images//permafrost_distribution_in_the_arctic.jpg]

Renssen, H., H. Seppa, X. Crosta, H. Goosse, and D.M. Roche, 2012: Global characterization of the Holocene Thermal Maximum. *Quat. Sci. Rev.*, **48**, 7-19.

Ruddiman, W.F, 2008: *Earth's Climate: Past and Future: 2nd Edition*. Freeman, W.H. & Company, New York, NY, 388 pp.

Schmidt, G.A., M. Kelley, L. Nazarenko, R. Ruedy, G.L. Russell, I. Aleinov, M. Bauer, S.E. Bauer, M.K. Bhat, R. Bleck, V. Canuto, Y.-H. Chen, Y. Cheng, T.L. Clune, A. Del Genio, R. de Fainchtein, G. Faluvegi, J.E. Hansen, R.J. Healy, N.Y. Kiang, D. Koch, A.A. Lacis, A.N. LeGrande, J. Lerner, K.K. Lo, E.E. Matthews, S. Menon, R.L. Miller, V. Oinas, A.O. Oloso, J.P. Perlwitz, M.J. Puma, W.M. Putman, D. Rind, A. Romanou, M. Sato, D.T. Shindell, S. Sun, R.A. Syed, N. Tausnev, K. Tsigaridis, N. Unger, A. Voulgarakis, M.-S. Yao, and J. Zhang, 2014: Configuration and assessment of the GISS ModelE2 contributions to the CMIP5 archive. *J. Adv. Model. Earth Syst.*, **6**, no. 1, 141-184, doi:10.1002/2013MS000265.

Serreze, M.C. and R.G. Barry, 2014: *The Arctic climate system*. Cambridge University Press, New York, NY, 415 pp.

Shur, Y.L. and M.T. Jorgenson, 2007: Patterns of Permafrost Formation and Degradation in Relation to Climate and Ecosystems. *Permafrost and Perigl. Proc.*, **18**, 7-18.

Taylor, K.E., G.A. Meehl, and R.J. Stouffer, 2012: An Overview of CMIP5 and the Experimental Design. *Bull. Amer. Met. Soc.*, **93**, 485-498.

Uppala, S.M., P.W. Kallberg, A.J. Simmons, U. Andrae, V. Da Costa Bechtold, M. Fiorino, J.K. Gibson, J. Haseler, A. Hernandez, G.A. Kelly, X. Li, K. Onogi, S. Saarinen, N. Sokka, R.P. Allan, E. Andersson, K. Arpe, M.A. Balmaseda, A.C.M. Beljaars, L. Van De Berg, J. Bidlot, N. Bormann, S. Caires, F. Chevallier, A. Dethof, M. Dragosavac, M. Fisher, M. Fuentes, S. Hagemann, E. Holm, B.J. Hoskins, L. Isaksen, P. A. E. M. Janssen, R. Jenne, A. P. McNally, J.-F. Mahfouf, J.-J. Morcrette, N. A. Rayner, R. W. Saunders, P. Simon, A. Sterl, K. E. Trenberth, A. Untch, D. Vasiljevic, P. Viterbo, and J. Woollen, 2005: The ERA-40 re-analysis. *Q.J.R. Met. Soc.*, **131**, 2961-3012.

Van Everdingen, R. (ed.): 1998. *Multi-Language Glossary of Permafrost and Related Ground-Ice Terms*, revised May 2005. National Snow and Ice Data Center/World Data Center for Glaciology, Boulder, CO, <http://nsidc.org/fgdc/glossary/>.

Viereck, L.A., and E.L. Little, 1972: *Alaska Trees and Shrubs*. Department of Agriculture, Washington D.C., 265 pp.

Walker, D. A., G. J. Jia, H. E. Epstein, M. K. Reynolds, F. S. Chapin Iii, C. Copass, L. D. Hinzman, J.A. Knudson, H.A. Maier, G.J. Michaelson, F.Nelson, C.L. Ping, V.E. Romanovsky, and N. Shiklomanov, 2003: Vegetation-soil-thaw-depth relationships along a low-arctic bioclimate gradient, Alaska: Synthesis of information from the ATLAS studies. *Permafrost and Perigl. Proc.* **14**,103-123.

Watanabe, S., T. Hajima, K. Sudo, T. Nagashima, T. Takemura, H. Okajima, T. Nozawa, H. Kawase, M. Abe, T. Tokohata, and T. Ise, 2011: MIROC-ESM 2010: model description and basic results of CMIP 5-20 c 3 m experiments. *Geosci. Mod. Dev.*, **4**, 845-872.

Yukimoto, Seiji, Yukimasa Adachi, Masahiro Hosaka, Tomonori Sakami, Hiromasa Yoshimura, Mikitoshi Hirabara, Taichu Y. Tanaka, E. Shindo, H. Tsujino, M. Deushi, and R. Mizuta, 2012: A new global climate model of the Meteorological Research Institute: MRI-CGCM3—model description and basic performance. *Journ. Met. Soc. Japan*, **90A**, 23-64.

